

PREPARED FOR SUBMISSION TO JCAP

Calculating the power spectrum in stochastic inflation by Monte Carlo simulation and least squares curve fitting

Koichi Miyamoto^a Yuichiro Tada^{b,c,d}

^aCenter for Quantum Information and Quantum Biology, The University of Osaka, Toyonaka 560-0043, Japan

^bDepartment of Physics, Rikkyo University, Toshima, Tokyo 171-8501, Japan

^cInstitute for Advanced Research, Nagoya University, Furo-cho, Chikusa-ku, Nagoya 464-8601, Japan

^dDepartment of Physics, Nagoya University, Furo-cho, Chikusa-ku, Nagoya 464-8602, Japan

E-mail: miyamoto.kouichi.qiqb@osaka-u.ac.jp, yuichiro.tada@rikkyo.ac.jp

Abstract. The stochastic- $\delta\mathcal{N}$ formalism is widely used to study inflation models in which the quantum diffusion of inflatons dominates the background dynamics, leading to interesting phenomena such as the production of primordial black holes. Among numerical approaches to calculate the curvature perturbation spectrum $\mathcal{P}_\zeta(k)$ in this formalism, the Monte Carlo simulation-based approach has been proposed as a promising choice, especially in multifield cases. In this approach, we generate many paths of inflatons from the initial points to the end of inflation, obtain statistics of $\delta\mathcal{N}$ from the paths, and then estimate $\mathcal{P}_\zeta(k)$. However, this method involves a nested Monte Carlo simulation, which requires generating many branch paths from each trunk path at the point corresponding to the scale k of interest, resulting in a high computational cost. In this paper, we propose a new Monte Carlo-based approach that utilizes least squares fitting, introducing two novel features for reducing computational cost. First, we devise a simple estimator of a key statistic $\langle\delta\mathcal{N}_\mathbf{x}^2\rangle$, the variance of $\delta\mathcal{N}$ conditioned on the branching point, to avoid nesting path generation. Second, via least squares fitting of a parametric function to the sampled values of the estimator, we obtain not just an estimate of $\mathcal{P}_\zeta(k)$ for a single value of k but an approximating function of $\mathcal{P}_\zeta(k)$ over a range of k of interest. We also conduct numerical demonstrations for concrete inflation models, which show the usefulness of our method.

Contents

1	Introduction	1
2	Preliminary	3
2.1	Stochastic inflation	3
2.2	Least squares curve fitting with noisy data	5
3	Proposed method	6
3.1	Naive method by nested Monte Carlo simulation	6
3.2	Method by unnested Monte Carlo simulation	8
3.3	Method by Monte Carlo simulation and least squares curve fitting	9
3.4	Relation of the adopted power spectrum formula to others	12
4	Numerical results	14
4.1	Chaotic inflation	14
4.2	Starobinsky’s linear-potential model	16
4.3	Flat quantum well	17
4.4	Hybrid inflation	20
5	Summary	21
A	Boundary shifting	21

1 Introduction

Inflation, the accelerated expansion of space in the early universe driven by certain scalar fields called inflatons, is a standard paradigm in cosmology. One of its virtues, along with solving the horizon and flatness problems, is that it produces primordial density perturbations, which result in structures in today’s universe, such as galaxies and clusters, through inflatons’ quantum fluctuations.

Among various approaches to analyzing the inflationary primordial perturbations, the δN formalism [1–5], which relates fluctuations of the e-fold number N during inflation in different spatial patches to primordial perturbations, is one of the standard ones. In particular, it is very helpful in the context of *stochastic inflation*. Stochastic inflation (see Refs. [6–16] for the first works and also Ref. [17] for a recent review) is a probabilistic formalism for long-wavelength modes of fields. It treats $\mathcal{X} = (\varphi, \varpi)$, inflatons and their conjugate momenta coarse-grained on a superHubble scale, and describes their stochastic time-evolution driven by quantum fluctuations with the Langevin equation. The distributions of the e-fold number and the large-scale primordial perturbation are accordingly determined.

This *stochastic- δN formalism* [18–22] has been used to study many interesting cosmological scenarios. In particular, it takes advantage when the ordinary linear perturbation analysis, which assumes that the background dynamics dominate the fluctuations, does not work well, e.g., in the diffusion-dominated scenario, where inflatons traverse a very flat region in their potential, and thus their stochastic movement dominates over the deterministic slow-roll. Such a scenario has attracted attention because amplitudes of the primordial curvature

perturbation ζ of the corresponding wavelengths can be amplified, which leads to various cosmological phenomena such as the production of primordial black holes, a candidate for dark matter. In fact, in analytical and numerical approaches, previous studies [23–56] have performed stochastic inflation-based analyses in aforementioned scenarios, aiming to calculate quantities related to cosmological phenomena and observations, such as the power spectrum $\mathcal{P}_\zeta(k)$, which represents the amplitude of primordial perturbations of scale k .

However, extending such analyses to general cases, especially multifield models, is practically challenging, although there are well-motivated multifield diffusion-dominated scenarios such as mild waterfall transition in hybrid inflation [19, 23, 50, 57, 58]. Since analytical approaches are basically applicable only to single-field cases, we often resort to numerical ones. A numerical approach that is seemingly appealing is the Monte Carlo simulation-based method proposed in Ref. [19], where we generate many paths of $\boldsymbol{\chi}$'s time-evolution from an initial point to the end of inflation (EOI) and use them to calculate statistical quantities such as $\mathcal{P}_\zeta(k)$. Since Monte Carlo simulation is often used to analyze high-dimensional random processes, avoiding the blow-up of the computational cost, this method seems a good choice in multifield cases. However, this method suffers from high computational cost, whether the inflation is single or multiple, because it requires *nested Monte Carlo simulation*, whose procedure is as follows. We first generate many paths. On each of them, we take points corresponding to k 's for which we want to calculate $\mathcal{P}_\zeta(k)$. Then, from these points, we generate many branch paths. The total number of paths including branches is of order $O(n_{\text{path},1}n_{\text{path},2}n_{\text{PS}})$, where $n_{\text{path},1}$ is the number of trunk paths, $n_{\text{path},2}$ is the branch number per branching point, and n_{PS} is the number of k 's.

In this paper, we propose a novel Monte Carlo-based method to calculate $\mathcal{P}_\zeta(k)$ built upon the formula given by Ando and Vennin (AV20) in Ref. [21]. Although we leave the detail to Secs. 2 and 3, according to the formula, we can find $\mathcal{P}_\zeta(k)$ via calculating $\left\langle \text{Var} \left[\mathcal{N}_{\boldsymbol{\chi}_{N_{\text{bk}}}} \mid \boldsymbol{\chi}_{N_{\text{bk}}} \right] \right\rangle$, the variance of the e-fold number of paths starting from $\boldsymbol{\chi}_{N_{\text{bk}}}$, $\boldsymbol{\chi}$ at the backward e-fold N_{bk} , averaged with respect to $\boldsymbol{\chi}_{N_{\text{bk}}}$. Here, the backward e-fold means the e-fold counted from the EOI along the path, and the value of N_{bk} has a one-to-one correspondence with k , the wavenumber of interest, in our algorithm. Since this is a kind of nested expectation, we are seemingly required to run a nested Monte Carlo simulation. Fortunately, as proposed in Sec. 3, we can take an estimator of $\text{Var} \left[\mathcal{N}_{\boldsymbol{\chi}_{N_{\text{bk}}}} \mid \boldsymbol{\chi}_{N_{\text{bk}}} \right]$ by $\frac{1}{2} \left(\mathcal{N}_{\boldsymbol{\chi}_{N_{\text{bk}}}}^{(1)} - \mathcal{N}_{\boldsymbol{\chi}_{N_{\text{bk}}}}^{(2)} \right)^2$, where $\mathcal{N}_{\boldsymbol{\chi}_{N_{\text{bk}}}}^{(1,2)}$ are the e-fold numbers of two paths that branch at backward e-fold N_{bk} . We can calculate this by generating just two branches at each branching point, which means that the number of paths immediately reduces. We further make an improvement on the computational cost with respect to n_{PS} , leveraging *least squares curve fitting*. On each trunk path, we generate two branches not from prefixed values of N_{bk} but from *one* randomly chosen value of N_{bk} . We then obtain a set of $\left(N_{\text{bk}}, \frac{1}{2} \left(\mathcal{N}_{\boldsymbol{\chi}_{N_{\text{bk}}}}^{(1)} - \mathcal{N}_{\boldsymbol{\chi}_{N_{\text{bk}}}}^{(2)} \right)^2 \right)$, and perform least squares fitting to this sample set, using some parametric function. This yields not the values of the power spectrum at a finite number of k but its *approximate function* over a range of scales. The number of paths generated in our method is just $O(n_{\text{path},1})$, which means a large reduction of the computational cost.

After presenting our method in full detail in Sec. 3, in Sec. 4, we perform its numerical demonstrations in four test cases. The first three are single-field models, for which the precise power spectrum is obtained by other methods, and thus, we can make a comparison to check our method. The last one is hybrid inflation, one of the multifield models, in which our

method is particularly desired. The results demonstrate that our method works in the tested cases to some extent.

2 Preliminary

2.1 Stochastic inflation

We consider the general relativistic system of $\phi = (\phi_1, \dots, \phi_d)$, d canonical scalar fields called inflatons,¹ described by the following action

$$S = \int d^4x \sqrt{-g} \left[\frac{1}{2} R - \frac{1}{2} \sum_{i=1}^d g^{\mu\nu} \partial_\mu \phi_i \partial_\nu \phi_i - V(\phi) \right], \quad (2.1)$$

where R is the Ricci scalar associated with the spacetime metric $g_{\mu\nu}$, $V(\phi)$ is the potential of ϕ , and we adopt the Planck unit where $c = \hbar = M_{\text{Pl}} = 1$ (M_{Pl} is the reduced Planck mass). With the use of the e-folds $N := \ln a$ defined by the scale factor a as the time variable and the flat slicing for the equal-time hypersurface,² we obtain the following Langevin equation that describes the time evolution of $\mathcal{X} := (\varphi, \varpi)$, the superHubble parts of ϕ and ϕ 's conjugate momenta $\pi := (\pi_1, \dots, \pi_n)$: for each $i = 1, \dots, d$,

$$\begin{aligned} \frac{d\varphi_i(N)}{dN} &= \frac{\varpi_i(N)}{H(\varphi(N), \varpi(N))} + \xi_{\phi_i}(N), \\ \frac{d\varpi_i(N)}{dN} &= -3\varpi_i(N) - \frac{\partial_{\phi_i} V(\varphi(N))}{H(\varphi(N), \varpi(N))} + \xi_{\pi_i}(N). \end{aligned} \quad (2.2)$$

$H := \dot{a}/a$ is the Hubble parameter given via the Friedmann equation

$$3H^2(\phi, \pi) = \frac{1}{2} \sum_{i=1}^d \pi_i^2(N) + V(\phi). \quad (2.3)$$

$\varphi = (\varphi_1, \dots, \varphi_d)$ and $\varpi = (\varpi_1, \dots, \varpi_d)$ are defined by coarse-graining:

$$\begin{aligned} \varphi_i(N, \mathbf{x}) &:= \int \frac{d^3k}{(2\pi)^3} e^{i\mathbf{k}\cdot\mathbf{x}} \tilde{\phi}_i(N, \mathbf{k}) \Theta(k_\sigma(N) - k), \\ \varpi_i(N, \mathbf{x}) &:= \int \frac{d^3k}{(2\pi)^3} e^{i\mathbf{k}\cdot\mathbf{x}} \tilde{\pi}_i(N, \mathbf{k}) \Theta(k_\sigma(N) - k). \end{aligned} \quad (2.4)$$

Here, $\tilde{\phi}_i(N, \mathbf{k}) := \int d^3x e^{-i\mathbf{k}\cdot\mathbf{x}} \phi_i(N, \mathbf{x})$ (resp. $\tilde{\pi}_i(N, \mathbf{k}) := \int d^3x e^{-i\mathbf{k}\cdot\mathbf{x}} \pi_i(N, \mathbf{x})$) is the Fourier mode of ϕ_i (resp. π_i) with wavenumber vector \mathbf{k} . Θ is the Heaviside function that takes $\Theta(z) = 1$ for $z > 0$ and 0 for $z < 0$.³ $k_\sigma(N)$ is defined by $k_\sigma(N) := \sigma a(N)H$ with the dimensionless and dimensionful parameters σ and H , which are set so that $k_\sigma(N) \ll$

¹We supposed the canonical kinetic term for the inflatons for simplicity. The stochastic formalism can be generalized to curved-target-space models; see Ref. [59].

²See, e.g., Refs. [60–62] for discussions about e-folding number as the time variable in the stochastic formalism.

³The consistent definition of $\Theta(z)$ at $z = 0$ requires a detailed discussion of the discretization of the path integral. See Refs. [63, 64].

$a(N)H(\varphi(N), \varpi(N))$ holds for typical sample paths in the range of N under consideration.⁴ In this paper, we set $\sigma = 0.1$ and $\mathbf{H} = H(\phi_{\text{ini}}, \pi_{\text{ini}})$, assuming that (ϕ, π) takes a globally equal initial value $(\phi_{\text{ini}}, \pi_{\text{ini}})$. ξ_X ($X = \phi_i$ or π_i) are the white Gaussian noises with zero means and covariances

$$\langle \xi_X(N) \xi_Y(N') \rangle = \mathcal{P}_{XY}(k_\sigma(N)) \delta(N - N'), \quad (2.5)$$

for $X, Y = \phi_i, \pi_i$, where the power spectrum \mathcal{P}_{XY} defined by

$$\langle \hat{X}_{\mathbf{k}} \hat{Y}_{\mathbf{k}'} \rangle = (2\pi)^3 \delta^{(3)}(\mathbf{k} + \mathbf{k}') \frac{2\pi^2}{k^3} \mathcal{P}_{XY}(k), \quad (2.6)$$

with the corresponding quantum operators $\hat{X}_{\mathbf{k}}$ and $\hat{Y}_{\mathbf{k}}$ in Fourier space. While $\langle \cdot \rangle$ represents the quantum average in Eq. (2.6), it denotes the ensemble average in Eq. (2.5) and hereafter. Note that although \mathcal{X} (and also ξ) takes different values at different spatial points \mathbf{x} , we have omitted \mathbf{x} in Eq. (2.2). This is because we will hereafter solve Eq. (2.2) without considering \mathbf{x} dependence, and regard each sample path as representing a realization of the time-evolving $\mathcal{X}(N)$ at one spatial point.

When we generate a sample path of \mathcal{X} , we need to discretize Eq. (2.2) in time by some method. In this paper, we adopt the Euler–Maruyama (EM) method [66] given as

$$\begin{aligned} \varphi_i(N + \Delta N) &= \varphi_i(N) + \frac{\varpi_i(N)}{H(\varphi(N), \varpi(N))} \Delta N + \mathcal{P}_\phi(N, \varphi(N), \varpi(N)) \Delta W_i, \\ \varpi_i(N + \Delta N) &= \varpi_i(N) + \left(-3\varpi_i(N) - \frac{\partial_{\phi_i} V(\varphi(N))}{H(\varphi(N), \varpi(N))} \right) \Delta N, \end{aligned} \quad (2.7)$$

where ΔN is the discretization step width, and ΔW_i is a number sampled from the normal distribution with zero mean and variance ΔN . Also, we neglected ξ_{π_i} as they are slow-roll suppressed in general.

Inflation occurs when the inflatons roll in the flat part of the potential, and the potential is dominant in the energy density, ending when the potential is no longer dominant. According to the δN formalism [1–5], the curvature perturbation is related to the fluctuation of the e-fold number that passed during inflation. Determining a hypersurface \mathcal{S}_{EOI} in \mathbb{R}^{2d} called the EOI surface, we define a random variable $\mathcal{N}_{\mathbf{X}}$ as a kind of first passage time: along with a path of \mathcal{X} generated by Eq. (2.2) with the initial point \mathbf{X} , $\mathcal{N}_{\mathbf{X}}$ is the first time that \mathcal{X} reaches \mathcal{S}_{EOI} . We also define

$$\delta \mathcal{N}_{\mathbf{X}} := \mathcal{N}_{\mathbf{X}} - \langle \mathcal{N}_{\mathbf{X}} \rangle. \quad (2.8)$$

Using this, AV20 [21] gives the formula for the curvature perturbation power spectrum $\mathcal{P}_\zeta(k)$, which represents the magnitude of ζ on scale k , as follows⁵

$$\mathcal{P}_\zeta(k) \simeq \int d\mathbf{X} \frac{\partial P_{\text{bk}}}{\partial N_{\text{bk}}} (N_{\text{bk}(k)}, \mathbf{X}) \langle \delta \mathcal{N}_{\mathbf{X}}^2 \rangle. \quad (2.9)$$

⁴The coarse-graining scale k_σ is often defined by $\sigma a(N)H(\varphi(N), \varpi(N))$ in the literature, but it requires a circular definition of φ and ϖ . In this work, we rather use a certain constant \mathbf{H} as a model parameter. It is less physical but can avoid the circular definition, and the original algorithm for the power spectrum proposed in Ref. [21] and adopted in this work anyway needs to suppose that the Hubble parameter is almost constant. See also footnote 3 of Ref. [65].

⁵Though AV20 [21] omitted the dependency on ϖ from their expression (3.12) for simplicity, our phase-space point \mathbf{X} in Eq. (2.9) includes both φ and ϖ as a more general formula.

Here, $P_{\text{bk}}(N_{\text{bk}}, \cdot)$ is the probability density function (PDF) at backward e-fold N_{bk} , that is, the PDF of \mathcal{X} at N_{bk} e-folds before the EOI. $N_{\text{bk}}(k) := -\log\left(\frac{k}{k_{\text{end}}}\right)$ is the backward e-fold at which the scale k exits the coarse-graining radius, and $k_{\text{end}} := k_{\sigma}(N_{\text{end}})$ denotes the coarse-graining scale at the EOI. Hereafter, we regard \mathcal{P}_{ζ} as a function of the backward e-fold N_{bk} , letting $\mathcal{P}_{\zeta}(N_{\text{bk}})$ be the value of Eq. (2.9) with $N_{\text{bk}}(k)$ replaced with N_{bk} .

2.2 Least squares curve fitting with noisy data

Fitting a dataset of multiple variables to learn the underlying function that describes their relationships is a ubiquitous problem in various fields [67]. In the latter part of this paper, we will consider a kind of such problem. Concretely, the problem of our interest is formulated as follows: let X be a real-valued random variable and Y be another random variable given as $Y = m(X) + E$, where $m : \mathbb{R} \rightarrow \mathbb{R}$ is an unknown function and E is the noise, that is, a real random variable with zero mean conditioned on X . Then, given a dataset consisting of N_{samp} independent samples $(X_1, Y_1), \dots, (X_{N_{\text{samp}}}, Y_{N_{\text{samp}}})$ from the joint probability distribution $\mu_{X,Y}$ of (X, Y) , find an approximation function \tilde{m} of m .

A common approach to this is least-squares fitting. We choose a family of functions $f : \mathbb{R} \times \mathbb{R}^{N_{\text{param}}} \rightarrow \mathbb{R}$, where the first argument x corresponds to X , the second one is a set of N_{param} tunable real parameters denoted by $\boldsymbol{\theta} = (\theta_1, \dots, \theta_{N_{\text{param}}})$, and f is sufficiently smooth with respect to every argument. Then, we minimize the sum of squared residuals

$$\boldsymbol{\theta}_{\min} := \underset{\boldsymbol{\theta}}{\operatorname{argmin}} \frac{1}{N_{\text{samp}}} \sum_{n=1}^{N_{\text{samp}}} (f(X_n, \boldsymbol{\theta}) - Y_n)^2, \quad (2.10)$$

and let $\tilde{m} := f(\cdot, \boldsymbol{\theta}_{\min})$ be an approximation of m . In this approach, even though Y has the noise E , we can obtain a good approximation function if we have a large number of data points and a suitable functional form. Under some assumptions,⁶ the expected error in the form of the averaged squared residual is bounded as follows:

$$\mathbb{E} \left[\int (\tilde{m}(x) - m(x))^2 \mu_X(dx) \right] \leq c \frac{\ln n}{n} + 2 \inf_{\boldsymbol{\theta}} \int (f(x, \boldsymbol{\theta}) - m(x))^2 d\mu_X(x), \quad (2.11)$$

where $\mathbb{E}[\cdot]$ denotes the expectation with respect to the randomness of samples, μ_X denotes the distribution of X , and c is a constant independent of n . For the details, see Theorem 11.5 in Ref. [67]. The first term corresponds to the statistical error, whose decay rate, except for the logarithmic factor, is of order $O(1/n)$ as is common in the Monte Carlo method. The second term corresponds to the fitting error, and to suppress this term, we need to choose a function family that fits the target function m well.

The best-fit parameter set $\boldsymbol{\theta}_{\min}$ estimated as Eq. (2.10) is a random variable due to the randomness of the dataset $\{(X_n, Y_n)\}_{n=1, \dots, N_{\text{samp}}}$. Under the linear approximation of f as a function of $\boldsymbol{\theta}$ around $\boldsymbol{\theta} = \boldsymbol{\theta}_*$, where

$$\boldsymbol{\theta}_* := \underset{\boldsymbol{\theta}}{\operatorname{argmin}} \int (f(x, \boldsymbol{\theta}) - y)^2 d\mu_{X,Y}(x, y), \quad (2.12)$$

⁶To be precise, although Theorem 11.5 in Ref. [67] assumes the boundedness of Y , that in the problem considered later, which is defined in Eq. (3.11), is not bounded. Hereafter, we simply assume that this does not affect the accuracy of the least squares approximation, assuming that for some sufficiently large $L > 0$, the probability that $|Y| > L$ is negligible. Besides, we do not consider the truncation of the approximation function, which is done in Theorem 11.5 in Ref. [67], assuming that we obtain a well-fitted function.

the covariance matrix C of $\boldsymbol{\theta}_{\min} = (\theta_{\min,1}, \dots, \theta_{\min,N_{\text{param}}})$ becomes [68]

$$C_{ij} = \text{Cov}[\theta_{\min,i}, \theta_{\min,j}] \simeq \sigma_{\text{res}}^2 ((J^T J)^{-1})_{ij}. \quad (2.13)$$

Here, J is the Jacobian matrix of f , a $N_{\text{samp}} \times N_{\text{param}}$ matrix with the (n, i) -th entry $J_{ni} = \frac{\partial f}{\partial \theta_i}(X_n, \boldsymbol{\theta}_*)$, and σ_{res}^2 is the variance of $f(X, \boldsymbol{\theta}_*) - Y$. In practice, $\boldsymbol{\theta}_*$ is unknown, and so we approximate J as \tilde{J} with the (n, i) -th entry $\tilde{J}_{ni} \simeq \frac{\partial f}{\partial \theta_i}(X_n, \boldsymbol{\theta}_{\min})$ and σ_{res}^2 as the sample variance $\tilde{\sigma}_{\text{res}}^2$ of $f(X_n, \boldsymbol{\theta}_{\min}) - Y_n$, assuming that the sample number is sufficiently large and $\boldsymbol{\theta}_{\min}$ is close to $\boldsymbol{\theta}_*$.

Given the approximate parameter covariance matrix $\tilde{C} := \tilde{\sigma}_{\text{res}}^2 (\tilde{J}^T \tilde{J})^{-1}$, we can estimate the error in the obtained approximating function $\tilde{m}(x)$ at a given point x as

$$\begin{aligned} \sqrt{\text{Var}[\tilde{m}(x)]} &\simeq \Delta m(x) \\ &:= \sqrt{(\nabla_{\boldsymbol{\theta}} f(x, \boldsymbol{\theta}_{\min}))^T \cdot \tilde{C} \cdot \nabla_{\boldsymbol{\theta}} f(x, \boldsymbol{\theta}_{\min})}, \end{aligned} \quad (2.14)$$

where $\nabla_{\boldsymbol{\theta}} f(x, \boldsymbol{\theta}_{\min})$ is a N_{param} -dimensional column vector with i -th entry $\frac{\partial f}{\partial \theta_i}(x, \boldsymbol{\theta}_{\min})$. Then, $\Delta m(x)$ is an estimate of the pointwise error of \tilde{m} , under the assumption that $\boldsymbol{\theta}_{\min}$ is sufficiently close to $\boldsymbol{\theta}_*$ and the fitting error is negligible.

In estimating the power spectrum of the inflationary perturbation, which we consider later, we also aim to obtain the approximation function \tilde{m}' of m' , the derivative of m . If f is differentiable with respect to the first argument x , we obtain \tilde{m}' just by differentiating \tilde{m} , that is, $\tilde{m}' := \frac{\partial f}{\partial x}(\cdot, \boldsymbol{\theta}_{\min})$. The error in \tilde{m}' is also estimated similarly to the above as

$$\Delta m'(x) = \sqrt{\left(\nabla_{\boldsymbol{\theta}} \frac{\partial f}{\partial x}(x, \boldsymbol{\theta}_{\min}) \right)^T \cdot \tilde{C} \cdot \nabla_{\boldsymbol{\theta}} \frac{\partial f}{\partial x}(x, \boldsymbol{\theta}_{\min})}. \quad (2.15)$$

3 Proposed method

3.1 Naive method by nested Monte Carlo simulation

Although \mathcal{P}_{ζ} is formally given by Eq. (2.9), evaluating it is another issue. AV20 [21] gives analytic evaluations in some simple inflation models, but in general models, especially multifield ones, we need to numerically calculate \mathcal{P}_{ζ} . Seeing Eq. (2.9) that involves the probability and the expectation, we naturally consider that we can use the Monte Carlo method to calculate it. However, naively applying the Monte Carlo method has an issue, which we now see before presenting the method we propose.

We see that

$$\mathcal{P}_{\zeta}(N_{\text{bk}}) \simeq \frac{dF_{\langle \delta \mathcal{N}^2 \rangle}}{dN_{\text{bk}}}(N_{\text{bk}}), \quad (3.2)$$

where we define

$$F_{\langle \delta \mathcal{N}^2 \rangle}(N_{\text{bk}}) := \int d\mathbf{X} P_{\text{bk}}(N_{\text{bk}}, \mathbf{X}) \langle \delta \mathcal{N}_{\mathbf{X}}^2 \rangle. \quad (3.3)$$

Approximating the N_{bk} derivative by the finite difference yields

$$\mathcal{P}_{\zeta}(N_{\text{bk}}) \simeq \frac{1}{2\Delta N_{\text{bk}}} (F_{\langle \delta \mathcal{N}^2 \rangle}(N_{\text{bk}} + \Delta N_{\text{bk}}) - F_{\langle \delta \mathcal{N}^2 \rangle}(N_{\text{bk}} - \Delta N_{\text{bk}})), \quad (3.4)$$

ALGORITHM 1. The naive method for calculating the power spectrum by the nested Monte Carlo simulation.

Input:

- $n_{\text{path},1}$: the number of sample paths
- $n_{\text{path},2}$: the number of branched sample paths
- \mathbf{X}_{ini} : the initial values of \mathcal{X}
- $N_{\text{bk},1}, \dots, N_{\text{bk},n_{\text{PS}}}$: n_{PS} values of N_{bk} at which $\mathcal{P}_{\zeta}(N_{\text{bk}})$ is calculated
- ΔN_{bk} : the width for the finite difference approximation of N_{bk} derivative

Output: $\tilde{\mathcal{P}}_{\zeta,i}$: approximate $\mathcal{P}_{\zeta}(N_{\text{bk},i})$ for $i = 1, \dots, n_{\text{PS}}$.

- 1: **for** $n = 1, \dots, n_{\text{path},1}$ **do**
- 2: Generate a path ω_n from \mathbf{X}_{ini} to the EOI based on Eq. (2.7).
- 3: **for** $m = 1, \dots, n_{\text{PS}}$ **do**
- 4: Let the values of \mathcal{X} at the backward e-folds $N_{\text{bk},m} \pm \Delta N_{\text{bk}}$ on ω_n be $\mathbf{X}_{\text{bk},n,m,\pm}$, respectively.
- 5: **for** $l = 1, \dots, n_{\text{path},2}$ **do**
- 6: Generate a path from $\mathbf{X}_{\text{bk},n,m,+}$ (resp. $\mathbf{X}_{\text{bk},n,m,-}$) to the EOI and let the elapsed e-fold $N_{n,m,l,+}$ (resp. $N_{n,m,l,-}$).
- 7: **end for**
- 8: Compute

$$V_{n,m,\pm} := \frac{1}{n_{\text{path},2}} \sum_{l=1}^{n_{\text{path},2}} N_{n,m,l,\pm}^2 - \left(\frac{1}{n_{\text{path},2}} \sum_{l=1}^{n_{\text{path},2}} N_{n,m,l,\pm} \right)^2. \quad (3.1)$$

- 9: **end for**
 - 10: **end for**
 - 11: **for** $m = 1, \dots, n_{\text{PS}}$ **do**
 - 12: Compute $F_m^{\pm} := \frac{1}{n_{\text{path},1}} \sum_{n=1}^{n_{\text{path},1}} V_{n,m,\pm}$.
 - 13: Output $\tilde{\mathcal{P}}_{\zeta,m} := \frac{1}{2\Delta N_{\text{bk}}} (F_m^+ - F_m^-)$
 - 14: **end for**
-

where the small displacement ΔN_{bk} is set appropriately. The problem thus boils down to calculating $F_{\langle \delta \mathcal{N}^2 \rangle}(N_{\text{bk}})$ for given N_{bk} . We note that this is a nested expectation calculation: $F_{\langle \delta \mathcal{N}^2 \rangle}(N_{\text{bk}})$ is the expectation of $\langle \delta \mathcal{N}_{\mathbf{X}}^2 \rangle$ with \mathbf{X} obeying the PDF $P_{\text{bk}}(N_{\text{bk}}, \cdot)$, and $\langle \delta \mathcal{N}_{\mathbf{X}}^2 \rangle$ is also an expectation. Then, we conceive the Monte Carlo-based algorithm 1 to calculate $\mathcal{P}_{\zeta}(N_{\text{bk}})$.

A brief explanation of this algorithm is as follows. Note that $\mathbf{X}_{\text{bk},n,m,\pm}$ in line 4 is a sample from the PDF $P_{\text{bk}}(N_{\text{bk}} \pm \Delta N_{\text{bk}}, \cdot)$. With this being \mathbf{X} , we generate samples of $\mathcal{N}_{\mathbf{X}}$ in line 6 and calculate $\langle \delta \mathcal{N}_{\mathbf{X}}^2 \rangle$ as a sample variance in line 8. Then, in line 12, we compute the average of these and let it be an approximation of $F_{\langle \delta \mathcal{N}^2 \rangle}(N_{\text{bk}} \pm \Delta N_{\text{bk}})$. This approach was, in fact, taken in the previous paper [19], where the author used a formula for \mathcal{P}_{ζ} slightly different from Eq. (2.9).

Although Algorithm 1 is straightforward, it has some shortcomings. First, it is a nested

Monte Carlo simulation and thus takes a long computational time. In the algorithm, updating \mathcal{X} by Eq. (2.7) is the computation that is iterated the most and is the most time-consuming. The total number of updates is evaluated as

$$O(n_{\text{path},1}n_{\text{path},2}n_{\text{PS}}n_t), \quad (3.5)$$

where $n_t := N_{\text{tot}}/\Delta N_{\text{bk}}$ is the typical number of time steps in a path and N_{tot} is the typical e-fold that elapses from the initial point to the EOI. Eq. (3.5) implies that the computational time becomes very long since it is proportional to the product of $n_{\text{path},1}$ and $n_{\text{path},2}$, which, to suppress the statistical error in Monte Carlo simulation, we need to set large. According to the well-known fact about the Monte Carlo method that for the statistical error at most ϵ , the required sample number is of order $O(1/\epsilon^2)$, we need to take $n_{\text{path},1}, n_{\text{path},2} = O(1/\epsilon^2)$, which makes Eq. (3.5) $O(1/\epsilon^4)$. In fact, in Ref. [19], both of them were set to 10^4 , whose product becomes 10^8 .

Another issue is that, as we see from Eq. (3.5) proportional to n_{PS} , the computational time becomes long if we want $\mathcal{P}_\zeta(N_{\text{bk}})$ for many values of N_{bk} , which is required for precise discussion on cosmological implications of the calculated power spectrum. Moreover, along with the statistical error, \mathcal{P}_ζ calculated by Eq. (3.4) contains the error by the finite difference approximation.

As we will see in the following, the method we propose solves these shortcomings of Algorithm 1.

3.2 Method by unnested Monte Carlo simulation

Now, let us see that we can avoid the nested Monte Carlo simulation by rewriting the formula (3.3) for $F_{\langle\delta\mathcal{N}^2\rangle}$. By a simple calculation, we see that

$$\langle\delta\mathcal{N}_{\mathbf{X}}^2\rangle = \left\langle \frac{1}{2} \left(\mathcal{N}_{\mathbf{X}}^{(1)} - \mathcal{N}_{\mathbf{X}}^{(2)} \right)^2 \right\rangle, \quad (3.6)$$

where $\mathcal{N}_{\mathbf{X}}^{(1)}$ and $\mathcal{N}_{\mathbf{X}}^{(2)}$ are two i.i.d. random variables with the same distribution as $\mathcal{N}_{\mathbf{X}}$. Thus, we can write Eq. (3.3) as

$$\begin{aligned} & F_{\langle\delta\mathcal{N}^2\rangle}(N_{\text{bk}}) \\ &= \int d\mathbf{X} \int_0^\infty dN_{\text{bk},1} \int_0^\infty dN_{\text{bk},2} P_{\text{bk}}(N_{\text{bk}}, \mathbf{X}) P_{\mathcal{N}_{\mathbf{X}}}(N_{\text{bk},1}) P_{\mathcal{N}_{\mathbf{X}}}(N_{\text{bk},2}) \frac{1}{2} (N_{\text{bk},1} - N_{\text{bk},2})^2, \end{aligned} \quad (3.7)$$

where $P_{\mathcal{N}_{\mathbf{X}}}$ is the PDF of $\mathcal{N}_{\mathbf{X}}$.

Having this formula, we conceive another Monte Carlo-based approach to calculate $F_{\langle\delta\mathcal{N}^2\rangle}(N_{\text{bk}})$: we sample many tuples $(\mathbf{X}, N_{\text{bk},1}, N_{\text{bk},2})$ from the joint PDF $P_{\text{joint}}(\mathbf{X}, N_{\text{bk},1}, N_{\text{bk},2}) := P_{\text{bk}}(N_{\text{bk}}, \mathbf{X}) P_{\mathcal{N}_{\mathbf{X}}}(N_{\text{bk},1}) P_{\mathcal{N}_{\mathbf{X}}}(N_{\text{bk},2})$ and take the sample average of $\frac{1}{2}(N_{\text{bk},1} - N_{\text{bk},2})^2$ as an approximation of $F_{\langle\delta\mathcal{N}^2\rangle}(N_{\text{bk}})$. The concrete procedure is given as Algorithm 2. This method avoids the nested Monte Carlo simulation, and its computational time is

$$O(n_{\text{path}}n_{\text{PS}}n_t). \quad (3.9)$$

However, it still gives the power spectrum only for preselected discrete values of N_{bk} and takes time proportional to n_{PS} , the number of values of N_{bk} . Additionally, the finite difference error persists.

ALGORITHM 2. The Monte Carlo-based method for calculating the power spectrum without the nested simulation.

Input:

- n_{path} : the number of sample paths
- \mathbf{X}_{ini} : the initial values of \mathcal{X}
- $N_{\text{bk},1}, \dots, N_{\text{bk},n_{\text{PS}}}$: n_{PS} values of N_{bk} at which $\mathcal{P}_{\zeta}(N_{\text{bk}})$ is calculated
- ΔN_{bk} : the width for the finite difference approximation of N_{bk} derivative

Output: $\tilde{\mathcal{P}}_{\zeta,i}$: approximate $\mathcal{P}_{\zeta}(N_{\text{bk},i})$ for $i = 1, \dots, n_{\text{PS}}$.

- 1: **for** $n = 1, \dots, n_{\text{path}}$ **do**
- 2: Generate a path ω_n from \mathbf{X}_{ini} to the EOI based on Eq. (2.7).
- 3: **for** $m = 1, \dots, n_{\text{PS}}$ **do**
- 4: Let the values of \mathcal{X} at the backward e-folds $N_{\text{bk},m} \pm \Delta N_{\text{bk}}$ on ω_n be $\mathbf{X}_{\text{bk},n,m,\pm}$, respectively.
- 5: Generate two paths from $\mathbf{X}_{\text{bk},n,m,+}$ (resp. $\mathbf{X}_{\text{bk},n,m,-}$) to the EOI and let the elapsed e-folds be $N_{n,m,1,+}$ and $N_{n,m,2,+}$ (resp. $N_{n,m,1,-}$ and $N_{n,m,2,-}$).
- 6: **end for**
- 7: **end for**
- 8: **for** $m = 1, \dots, n_{\text{PS}}$ **do**
- 9: Compute

$$\tilde{F}_m^{\pm} := \frac{1}{n_{\text{path}}} \sum_{n=1}^{n_{\text{path}}} \frac{1}{2} (N_{n,m,1,\pm} - N_{n,m,2,\pm})^2. \quad (3.8)$$

- 10: Output $\tilde{\mathcal{P}}_{\zeta,m} := \frac{1}{2\Delta N_{\text{bk}}} (F_m^+ - F_m^-)$
 - 11: **end for**
-

3.3 Method by Monte Carlo simulation and least squares curve fitting

We now present our main proposal, which involves calculating the power spectrum using a Monte Carlo simulation and least squares curve fitting.

We aim to find a function $\tilde{F}_{\langle \delta \mathcal{N}^2 \rangle}(N_{\text{bk}})$ that well fits $F_{\langle \delta \mathcal{N}^2 \rangle}(N_{\text{bk}})$ over some range $[N_{\text{bk},l}, N_{\text{bk},u}]$ of N_{bk} that we are interested in. To do so, we consider this task as a kind of problem described in Sec. 2.2. We view a random variable \mathcal{N}_{bk} that uniformly distributes in $[N_{\text{bk},l}, N_{\text{bk},u}]$ as X and

$$Y_{\langle \delta \mathcal{N}^2 \rangle} := \frac{1}{2} \left(\mathcal{N}_{\text{bk}}^{(1)} - \mathcal{N}_{\text{bk}}^{(2)} \right)^2. \quad (3.11)$$

as Y . Here, \mathcal{X}_{bk} is a \mathbb{R}^{2d} -valued random variable such that the joint distribution of $(\mathcal{N}_{\text{bk}}, \mathcal{X}_{\text{bk}})$ has the PDF

$$P_{\mathcal{N}_{\text{bk}}, \mathcal{X}_{\text{bk}}}(N_{\text{bk}}, \mathbf{X}_{\text{bk}}) = P_{\mathcal{N}_{\text{bk}}}(N_{\text{bk}}) P_{\text{bk}}(N_{\text{bk}}, \mathbf{X}_{\text{bk}}), \quad (3.12)$$

ALGORITHM 3. The proposed method for finding an approximation function of the power spectrum by Monte Carlo simulation and least squares fitting (MCLSFit).

Input:

- n_{path} : the number of sample paths
- \mathbf{X}_{ini} : the initial values of \mathcal{X}
- $[N_{\text{bk},l}, N_{\text{bk},u}]$: the range of the backward e-fold on which the power spectrum is approximated
- $f(N_{\text{bk}}, \boldsymbol{\theta})$: the real-valued function that has the parameters $\boldsymbol{\theta}$ and is differentiable with N_{bk}

Output: Functions $\tilde{F}_{\langle\delta N^2\rangle}$ and $\tilde{\mathcal{P}}_\zeta$ that approximate $F_{\langle\delta N^2\rangle}$ and \mathcal{P}_ζ , respectively.

- 1: **for** $n = 1, \dots, n_{\text{path}}$ **do**
- 2: Sample a value $N_{\text{bk},n}$ from $U(N_{\text{bk},l}, N_{\text{bk},u})$, the uniform distribution with support $[N_{\text{bk},l}, N_{\text{bk},u}]$.
- 3: Generate a path ω_n from \mathbf{X}_{ini} to the EOI based on Eq. (2.7).
- 4: Let the value of \mathcal{X} at the backward e-fold $N_{\text{bk},n}$ on ω_n be $\mathbf{X}_{\text{bk},n}$.
- 5: Generate two paths from $\mathbf{X}_{\text{bk},n}$ to the EOI and let the elapsed e-folds be $N_{n,1}$ and $N_{n,2}$.
- 6: **end for**
- 7: Find

$$\boldsymbol{\theta}_{\min} := \underset{\boldsymbol{\theta}}{\operatorname{argmin}} \sum_{n=1}^{n_{\text{path}}} \left[f(N_{\text{bk},n}, \boldsymbol{\theta}) - \frac{1}{2} (N_{n,1} - N_{n,2})^2 \right]^2. \quad (3.10)$$

- 8: Output $f(\cdot, \boldsymbol{\theta}_{\min})$ and $\partial_{N_{\text{bk}}} f(\cdot, \boldsymbol{\theta}_{\min})$ as $\tilde{F}_{\langle\delta N^2\rangle}$ and $\tilde{\mathcal{P}}_\zeta$, respectively.
-

where

$$P_{\mathcal{N}_{\text{bk}}}(N_{\text{bk}}) := \begin{cases} \frac{1}{N_{\text{bk},u} - N_{\text{bk},l}} & ; N_{\text{bk},l} \leq N_{\text{bk}} \leq N_{\text{bk},u} \\ 0 & ; \text{otherwise} \end{cases} \quad (3.13)$$

is the PDF of \mathcal{N}_{bk} . $\mathcal{N}_{\mathbf{x}_{\text{bk}}}^{(1)}$ and $\mathcal{N}_{\mathbf{x}_{\text{bk}}}^{(2)}$ are i.i.d. random variables, each of which, conditioned that $\mathbf{x}_{\text{bk}} = \mathbf{X}_{\text{bk}}$, has the same PDF as $\mathcal{N}_{\mathbf{X}_{\text{bk}}}$. Now, we decompose Y as $Y = m(\mathcal{N}_{\text{bk}}) + E$ with

$$\begin{aligned} m(\mathcal{N}_{\text{bk}}) &= F_{\langle\delta \mathcal{N}^2\rangle}(\mathcal{N}_{\text{bk}}), \\ E &= \frac{1}{2} \left(\mathcal{N}_{\mathbf{x}_{\text{bk}}}^{(1)} - \mathcal{N}_{\mathbf{x}_{\text{bk}}}^{(2)} \right)^2 - F_{\langle\delta \mathcal{N}^2\rangle}(\mathcal{N}_{\text{bk}}). \end{aligned} \quad (3.14)$$

By definition,

$$\mathbb{E}[E \mid \mathcal{N}_{\text{bk}} = N_{\text{bk}}] = 0, \quad (3.15)$$

holds. Thus, the current task matches the problem setting in Sec. 2.2, and we can find an approximating function $\tilde{F}_{\langle\delta \mathcal{N}^2\rangle}(N_{\text{bk}})$ of $F_{\langle\delta \mathcal{N}^2\rangle}(N_{\text{bk}})$ by the method described there: we generate sample values $\{(N_{\text{bk},n}, Y_{\langle\delta \mathcal{N}^2\rangle,n})\}_{n=1,\dots,n_{\text{path}}}$ of $(\mathcal{N}_{\text{bk}}, Y_{\langle\delta \mathcal{N}^2\rangle})$ and perform the least squares fit to the sample set. The concrete procedure, which we hereafter call MCLSFit, is described in Algorithm 3.

The resultant function $\tilde{F}_{\langle\delta\mathcal{N}^2\rangle}$ satisfies that

$$\begin{aligned} \mathbb{E} \left[\int_{N_{\text{bk},l}}^{N_{\text{bk},u}} \left(\tilde{F}_{\langle\delta\mathcal{N}^2\rangle}(N_{\text{bk}}) - F_{\langle\delta\mathcal{N}^2\rangle}(N_{\text{bk}}) \right)^2 \frac{dN_{\text{bk}}}{N_{\text{bk},u} - N_{\text{bk},l}} \right] \\ \leq c \frac{\ln n_{\text{path}}}{n_{\text{path}}} + 2 \inf_{\boldsymbol{\theta}} \int_{N_{\text{bk},l}}^{N_{\text{bk},u}} \left(f(N_{\text{bk}}, \boldsymbol{\theta}) - F_{\langle\delta\mathcal{N}^2\rangle}(N_{\text{bk}}) \right)^2 \frac{dN_{\text{bk}}}{N_{\text{bk},u} - N_{\text{bk},l}}. \end{aligned} \quad (3.16)$$

We now avoid not only the nested Monte Carlo simulation but also the n_{PS} -times iterations: the computational time is

$$O(n_{\text{path}} n_t). \quad (3.17)$$

We have a function $\tilde{F}_{\langle\delta\mathcal{N}^2\rangle}$ that approximately gives $F_{\langle\delta\mathcal{N}^2\rangle}$ for any $N_{\text{bk}} \in [N_{\text{bk},l}, N_{\text{bk},u}]$, not the values at a finite number of preselected N_{bk} . Besides, if $f(N_{\text{bk}}, \boldsymbol{\theta})$ is differentiable with respect to N_{bk} , we also have an approximation function $\tilde{P}_{\zeta} = d\tilde{F}_{\langle\delta\mathcal{N}^2\rangle}/dN_{\text{bk}}$ of the power spectrum P_{ζ} , which does not rely on the finite difference approximation. Moreover, if $f(N_{\text{bk}}, \boldsymbol{\theta})$ is differentiable with respect to $\boldsymbol{\theta}$, we can estimate the error in $\tilde{F}_{\langle\delta\mathcal{N}^2\rangle}$ and \tilde{P}_{ζ} as described in Sec. 2.2.

An issue is choosing a suitable function $f(N_{\text{bk}}, \boldsymbol{\theta})$ that can be fitted to $F_{\langle\delta\mathcal{N}^2\rangle}$ well. As is common in any machine learning problem, we should have some prior knowledge about the fitted function $F_{\langle\delta\mathcal{N}^2\rangle}$ in certain ways, such as qualitative discussions and approximate analyses, and reflect it onto f . In fact, in some of the test cases considered in Sec. 4, we use qualitative knowledge to choose f . If we do not have enough knowledge, the following way using the samples $\{(N_{\text{bk},n}, N_{n,1}, N_{n,2})\}_n$ would be helpful: we bin the samples based on N_{bk} and take an average of $\frac{1}{2}(N_1 - N_2)^2$ in each bin. This helps us roughly grasp the shape of \mathcal{P}_{ζ} and get guidance on choosing the fitting function. This can also be used to check the fitting quality afterward, even if we have plausible fitting functions. The concrete procedure of this method, which we hereafter call MCBinAve, is as shown in Algorithm 4.

We can regard \tilde{F}_m in Algorithm 4 as a Monte Carlo estimation of

$$\overline{F}(N_{\text{bk}}) := \frac{1}{\Delta N_{\text{bin}}} \int_{N_{\text{bk}} - \frac{1}{2}\Delta N_{\text{bin}}}^{N_{\text{bk}} + \frac{1}{2}\Delta N_{\text{bin}}} F_{\langle\delta\mathcal{N}^2\rangle}(N_{\text{bk}}) dN_{\text{bk}}, \quad (3.19)$$

the average of $F_{\langle\delta\mathcal{N}^2\rangle}$ over the bin, and $\tilde{\mathcal{P}}_{\zeta,m}$ as that of

$$\overline{\mathcal{P}}_{\zeta}(N_{\text{bk}}) := \frac{\overline{F}(N_{\text{bk}} + \frac{1}{2}\Delta N_{\text{bin}}) - \overline{F}(N_{\text{bk}} - \frac{1}{2}\Delta N_{\text{bin}})}{\Delta N_{\text{bin}}}, \quad (3.20)$$

the finite-difference approximation of the derivative of \overline{F} . The standard errors of these estimations are calculated as

$$\Delta \tilde{F}_m := \frac{1}{\sqrt{M_m}} \left(\frac{1}{M_m} \sum_{n=1}^{n_{\text{path}}} \frac{1}{4} (N_{n,1} - N_{n,2})^4 \mathbf{1}_{N_{\text{bin},m-1} \leq N_{\text{bk},n} < N_{\text{bin},m}} - \tilde{F}_m^2 \right)^{1/2}, \quad (3.21)$$

and

$$\Delta \tilde{\mathcal{P}}_{\zeta,m} := \frac{\sqrt{(\Delta \tilde{F}_m)^2 + (\Delta \tilde{F}_{m+1})^2}}{\Delta N_{\text{bin}}}. \quad (3.22)$$

ALGORITHM 4. The proposed method for finding an approximation of the power spectrum by binning and averaging the Monte Carlo samples (MCBinAve).

Input:

- n_{path} : the number of sample paths
- \mathbf{X}_{ini} : the initial values of \mathcal{X}
- $[N_{\text{bk},l}, N_{\text{bk},u}]$: the range of the backward e-fold on which the power spectrum is approximated
- n_{bin} : the number of bins

- 1: Run steps 1–6 in Algorithm 3.
- 2: Set $N_{\text{bin},m} := N_{\text{bk},l} + m\Delta N_{\text{bin}}$ with $\Delta N_{\text{bin}} := (N_{\text{bk},u} - N_{\text{bk},l})/n_{\text{bin}}$ for $m = 0, \dots, n_{\text{bin}}$.
- 3: **for** $m = 1, \dots, n_{\text{bin}}$ **do**
- 4: Compute

$$\tilde{F}_m := \frac{1}{M_m} \sum_{n=1}^{n_{\text{path}}} \frac{1}{2} (N_{n,1} - N_{n,2})^2 \mathbf{1}_{N_{\text{bin},m-1} \leq N_{\text{bk},n} < N_{\text{bin},m}}, \quad (3.18)$$

where the indicator function $\mathbf{1}_C$ takes 1 if the condition C holds and 0 otherwise, and $M_m := \sum_{n=1}^{n_{\text{path}}} \mathbf{1}_{N_{\text{bin},m-1} \leq N_{\text{bk},n} < N_{\text{bin},m}}$.

- 5: **end for**
 - 6: **for** $m = 1, \dots, n_{\text{bin}} - 1$ **do**
 - 7: Output $\tilde{\mathcal{P}}_{\zeta,m} := \frac{\tilde{F}_{m+1} - \tilde{F}_m}{\Delta N_{\text{bin}}}$ as an approximation of $\mathcal{P}_{\zeta}(N_{\text{bin},m})$.
 - 8: **end for**
-

3.4 Relation of the adopted power spectrum formula to others

Before moving to the concrete examples, we mention the difference in the variants of the power spectrum formula (2.9) proposed so far in the literature. While AV20 relates the scale of interest k with the phase-space point \mathbf{X} by the backward e-folds $N_{\text{bk}}(k) := -\ln(k/k_{\text{end}})$ from EOI, the original stochastic- $\delta\mathcal{N}$ approach by Fujita, Kawasaki, Tada, and Takesako (FKTT) [18, 19] chose the point \mathbf{X} from which the average e-folds to EOI, $\langle \mathcal{N}(\mathbf{X}) \rangle$, equal to $-\ln(k/k_{\text{end}})$. In the latest formulation by Animalì and Vennin (AV24) where the consistency between the two-point function and the spatial coarse-graining is carefully investigated, it is found that the FKTT formula was incidentally not a bad approximation in the large-volume limit $k \ll k_{\text{end}}$, though the average should be volume-weighted: the variance $\langle \delta\mathcal{N}_{\mathbf{X}}^2 \rangle$ should be replaced by

$$\langle \delta\mathcal{N}_{\mathbf{X}}^2 \rangle_V := \frac{\langle e^{3\mathcal{N}_{\mathbf{X}}} \mathcal{N}_{\mathbf{X}}^2 \rangle}{\langle e^{3\mathcal{N}_{\mathbf{X}}} \rangle} - \left(\frac{\langle e^{3\mathcal{N}_{\mathbf{X}}} \mathcal{N}_{\mathbf{X}} \rangle}{\langle e^{3\mathcal{N}_{\mathbf{X}}} \rangle} \right)^2, \quad (3.23)$$

and the scale is related to the point so that

$$\left(\frac{k_{\text{end}}}{2k} \right)^3 = \langle e^{3\mathcal{N}_{\mathbf{X}}} \rangle, \quad (3.24)$$

where the factor two reflects the fact that k should correspond not to the diameter but to the radius of the patch of interest. All these formulations of the power spectrum are summarized

in the following expression:

$$\mathcal{P}_\zeta(k) \simeq \int d\mathbf{X} \frac{\partial P_k(\mathbf{X})}{\partial(-\ln k)} \langle\langle \delta\mathcal{N}_{\mathbf{X}}^2 \rangle\rangle. \quad (3.25)$$

Here, $P_k(\mathbf{X})$ is the PDF of \mathbf{X} on a certain hypersurface corresponding to the scale k , as summarized by

$$P_k(\mathbf{X}) = \begin{cases} P(\mathbf{X} \mid \langle\mathcal{N}_{\mathbf{X}}\rangle = -\ln(k/k_{\text{end}})) & \text{for FKTT,} \\ P_{\text{bk}}(N_{\text{bk}}(k), \mathbf{X}) & \text{for AV20,} \\ P(\mathbf{X} \mid \langle e^{3\mathcal{N}_{\mathbf{X}}} \rangle = (k_{\text{end}}/(2k))^3) & \text{for AV24.} \end{cases} \quad (3.26)$$

$\langle\langle \delta\mathcal{N}_{\mathbf{X}}^2 \rangle\rangle$ represents the standard variance $\langle\delta\mathcal{N}_{\mathbf{X}}^2\rangle$ for FKTT and AV20, and the volume-weighted one $\langle\delta\mathcal{N}_{\mathbf{X}}^2\rangle_V$ for AV24. Their differences are higher-order in $\delta\mathcal{N}$ and hence the curvature perturbation, so they are expected not to be significant if $\mathcal{P}_\zeta(k) \ll 1$ as in a realistic model and most examples we will see below. Only the flat quantum well model in our examples can achieve $\mathcal{P}_\zeta > 1$ (see Fig. 6 of AV20 [21]) and exhibits a characteristic “leakage” feature from small-scale perturbations to large-scale ones. This feature is indeed predicted only in the AV20 formula because the surface condition $\langle\mathcal{N}_{\mathbf{X}}\rangle = -\ln(k/k_{\text{end}})$ in FKTT or $\langle e^{3\mathcal{N}_{\mathbf{X}}} \rangle = (k_{\text{end}}/(2k))^3$ in AV24 uniquely determines the corresponding inflaton value φ_* . We will come back to this point in Sec. 4.3, but we will merely focus on reproducing the AV20 result in the least squares fitting method without discussing the validity of this feature.

Let us also mention other approaches to computing the power spectrum in the stochastic formalism. One is the adjoint Fokker–Planck approach [50] as a kind of derivative of FKTT. There, the average $\langle\mathcal{N}_{\mathbf{X}}\rangle$ and the variance $\langle\delta\mathcal{N}_{\mathbf{X}}^2\rangle$ are calculated as functions of the phase-space point \mathbf{X} via the adjoint Fokker–Planck partial differential equation (PDE) proposed in Ref. [20] rather than the Monte Carlo way. While the Monte Carlo approach cannot calculate the variance smaller than the discretization step square, $(\Delta N)^2$, of the Langevin equation (Eq. (2.7)), the PDE approach is free from such a limitation. On the other hand, numerical solvers for PDEs in general suffer from the *curse of dimensionality*, i.e., the exponential complexity in the number of fields d (or $2d$ for phase space). They are hence complementary to each other.

The lattice implementation of the stochastic formalism, dubbed *STOchastic LAttice Simulation (STOLAS)* in Ref. [65], is a more direct approach compared to the derivatives of FKTT. As it literally simulates the spatial distribution of the curvature perturbation, the power spectrum (and beyond, such as the bispectrum and trispectrum, in principle) can be obtained by simply Fourier-transforming the real-space distribution. The calculable e-fold range $N_{\text{bk,u}} - N_{\text{bk,l}}$ (within one simulation) is limited by the lattice resolution. In the latest implementation [69], the single 256^3 -lattice simulation corresponding to $N_{\text{bk,u}} - N_{\text{bk,l}} \simeq \ln 256 \simeq 5.5$ takes 10 minutes in addition to 6 minutes for noise map generation (by MacBook Pro with Apple M1 Max CPU (10 cores), 64 GB RAM, and no GPU use)).

Another numerical simulation of stochastic inflation is FOrtran Recursive Exploration of Stochastic Trees (FOREST) by Ref. [70]. It computes the spatial correlation of the curvature perturbation as “stochastic trees”, which simulate the branching of Hubble patches. Though it is not explicitly given in the reference, it is expected to have the ability to calculate the power spectrum.

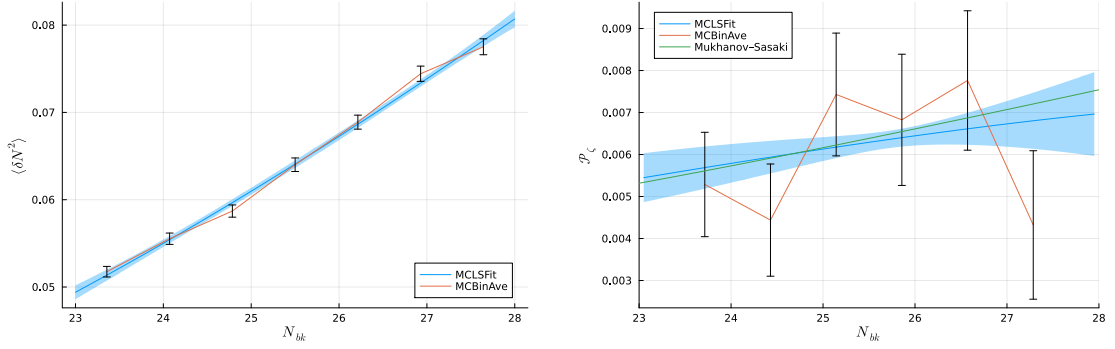


Figure 1. The approximating function of $F_{\langle \delta N^2 \rangle}$ (resp. \mathcal{P}_ζ) in chaotic inflation output by MCLSFIt is shown in the left panel (resp. the right panel) as a blue curve with the error shown as a blue band. The estimations by MCBinAve with 7 bins are shown as red curves with the error bars. All the errors are of 1σ level. In the right panel, \mathcal{P}_ζ calculated via solving the MS equation, is also shown in green.

4 Numerical results

We now conduct numerical demonstrations to run the proposed algorithms in four test cases. The first three are single-field models, for each of which the curvature perturbation power spectrum can be obtained at least approximately using existing methods. Although these models may not require our Monte Carlo-based methods, we can still compare our results with those of existing methods to assess the effectiveness of our approach. The last one is a multi-field model, for which existing approaches are more challenging than single-field cases, and it is the very situation where our method becomes helpful.

We use `DifferentialEquations.jl` [71] to generate paths according to Eq. (2.7), adopting the EM scheme with time step size $\Delta N = 0.01$ and setting the number of paths to $n_{\text{path}} = 10^5$, unless otherwise specified. Our code is available at <https://github.com/Koichi-Miyamoto/StochasticInflationMCLS>. All the calculations below were run on Fujitsu LIFEBOOK WP1/J3 with Intel Core Ultra 7 155H CPU (16 cores, 3.0 GHz), 32 GB RAM, and no GPU use.

4.1 Chaotic inflation

First, we consider the single-field chaotic inflation [72], where the potential is given by

$$V(\phi) = \frac{1}{2}m^2\phi^2, \quad (4.1)$$

with the inflaton mass m . We set the model parameters as $m = 0.0211$, $\phi_{\text{ini}} = 11$, and $\pi_{\text{ini}} = -\sqrt{\frac{2}{3}}m$, and define the EOI surface by $\epsilon_H = 0.3$,⁷ where

$$\epsilon_H := -\frac{\dot{H}(\varphi, \varpi)}{H^2(\varphi, \varpi)} = \frac{3}{2} \frac{\varpi^2}{\frac{1}{2}\varpi^2 + V(\varphi)}. \quad (4.2)$$

⁷Note that $\epsilon_H = 0.3$ means that inflation is still occurring. Nevertheless, we can set the EOI surface like this because the inflatons' dynamics has been well converged to the slow-roll attractor at this point and thus δN generated afterward is negligible. A similar discussion validates the choice of the EOI surface in Starobinsky's linear potential model too.

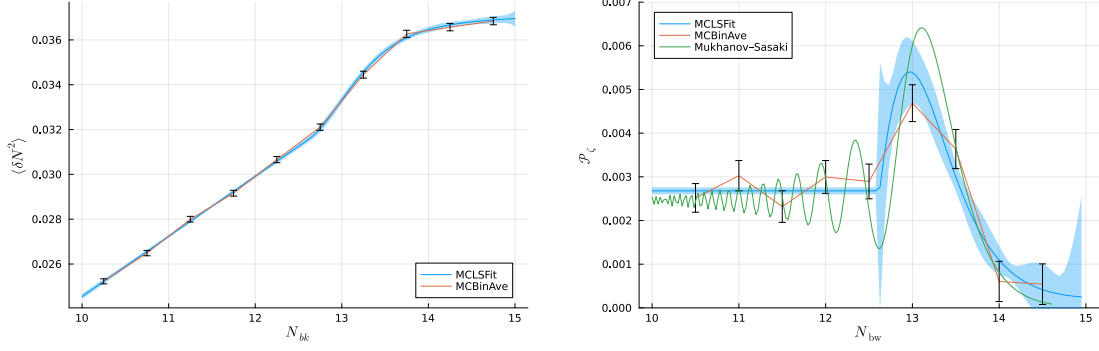


Figure 2. The same figure as FIG. 1 but for Starobinsky’s linear-potential model. The number of bins in MCBinAve is now 10.

This case falls into the ordinary slow-roll case, and thus the standard MS equation-based linear perturbation analysis is applicable. We can compare the result of our method with the MS-based result. The power spectrum of the inflaton’s noise is calculated up to the next-to-leading order in the slow-roll approximation as [65]

$$\mathcal{P}_\phi(N, \varphi) = \left(\frac{H}{2\pi}\right)^2 \left(\frac{\sigma H}{2H}\right)^{-6\epsilon_V + 2\eta_V} [1 + \epsilon_V(10 - 6\gamma - 12\ln 2) - 2\eta_V(2 - \gamma - 2\ln 2)], \quad (4.3)$$

where γ is Euler’s constant and the slow-roll parameters ϵ_V and η_V are defined as

$$\epsilon_V = \frac{1}{2} \left(\frac{V'(\varphi)}{V(\varphi)}\right)^2, \quad \eta_V = \frac{V''(\varphi)}{V(\varphi)}. \quad (4.4)$$

In our method, N_{bk} is sampled between $N_{bk,l} = 23$ and $N_{bk,u} = 28$. We take the following fitting function

$$f(N_{bk}, \boldsymbol{\theta}) = \exp \left(\sum_{\ell=0}^L \theta_\ell p_\ell \left(\frac{2N_{bk} - N_{bk,u} - N_{bk,l}}{N_{bk,u} - N_{bk,l}} \right) \right), \quad (4.5)$$

where p_ℓ is the ℓ -th Legendre polynomial and $L = 2$. This choice, an exponential function with a polynomial inside, is compatible with our knowledge that in the slow-roll approximation, $\mathcal{P}_\zeta(k)$ takes a power-law form: $\mathcal{P}_\zeta(k) \simeq A k^{n_s-1}$ with constants A and n_s . To tune $\boldsymbol{\theta}$, we use `LsqFit.jl` [73], which will also be used later.

The results of our methods MCLSFit and MCBinAve are shown in FIG. 1 along with 1σ -level standard errors, the doubles of Eqs. (2.14), (2.15), (3.21), and (3.22). For $\langle \delta \mathcal{N}^2 \rangle$, the results of MCLSFit and MCBinAve match well, which implies that the least squares fit is working. Regarding the power spectrum, the MCLSFit result fits the MS-based one, demonstrating that the proposed method as a whole is working well. The MCBinAve result looks non-smooth due to the statistical error, but it still roughly fits the MCLSFit and MS-based one. Generating the samples $\{(N_{n,1}, N_{n,2})\}_n$, which is the most time-consuming part in both MCLSFit and MCBinAve, took 8.5 minutes.

4.2 Starobinsky's linear-potential model

The next example is Starobinsky's linear-potential model [74], a single-field model with the following potential

$$V(\phi) = \begin{cases} V_0 + A_+(\phi - \phi_0) & \text{for } \phi \geq \phi_0, \\ V_0 + A_-(\phi - \phi_0) & \text{for } \phi \leq \phi_0, \end{cases} \quad (4.6)$$

where V_0 and A_{\pm} are positive parameters and ϕ_0 is a kink of the potential. We now consider the case that $A_+ > A_-$ and the inflaton rolls down from $\phi_{\text{ini}} > \phi_0$. In this case, the inflaton's terminal velocity in the region $\phi > \phi_0$ is larger than that in the region $\phi < \phi_0$. As a result, the inflaton undergoes the friction-dominated phase called ultra-slow-roll (USR) for a while after passing ϕ_0 , leading to the amplification of the curvature perturbation. The inflaton's noise power spectrum \mathcal{P}_ϕ is well approximated by $\mathcal{P}_\phi^{1/2} = \frac{H}{2\pi}$ when $\phi > \phi_0$. In the second phase, $\phi < \phi_0$, the following approximation formula is known in the constant-Hubble approximation [75]:

$$\begin{aligned} & \mathcal{P}_\phi(N, \varphi, \varpi) \\ &= \left(\frac{H_0}{2\pi}\right)^2 \times \frac{1}{2\alpha^6 \Lambda^2 \sigma^6} \left[3(\Lambda^2(\alpha^4(4\alpha - 7)\sigma^6 + \alpha^3(7\alpha - 16)\sigma^4 + (3 - 12\alpha)\sigma^2 - 3) \right. \\ & \quad + \Lambda(2(5 - 2\alpha)\alpha^4\sigma^6 + 2(14 - 5\alpha)\alpha^3\sigma^4 + 6(4\alpha - 1)\sigma^2 + 6) \\ & \quad - 3(\alpha^4\sigma^6 - (\alpha - 4)\alpha^3\sigma^4 + (4\alpha - 1)\sigma^2 + 1)) \cos(2(\alpha - 1)\sigma) \\ & \quad + (\sigma^2 + 1) \left(-18\Lambda(\alpha^2\sigma^2 + 1)^2 + 9(\alpha^2\sigma^2 + 1)^2 + \Lambda^2(2\alpha^6\sigma^6 + 9\alpha^4\sigma^4 + 18\alpha^2\sigma^2 + 9) \right) \\ & \quad + 6\sigma(\alpha^5(\Lambda - 1)\Lambda\sigma^4(\sigma^2 - 1) + \alpha^4(7\Lambda^2 - 10\Lambda + 3)\sigma^4 - \alpha^3(4\Lambda^2 - 7\Lambda + 3)\sigma^2(\sigma^2 - 1) \\ & \quad \left. - 3\alpha(\Lambda - 1)^2(\sigma^2 - 1) - 3(\Lambda - 1)^2\right) \sin(2\sigma - 2\alpha\sigma) \Big], \end{aligned} \quad (4.7)$$

Here, H_0 is the Hubble parameter at the initial time, $\Lambda := A_+/A_-$, and $\alpha := \exp(N - \mathcal{N}_0)$ with the transition time \mathcal{N}_0 defined as $\varphi(\mathcal{N}_0) = \phi_0$, which is also a random variable different among paths. Now, the model parameters are set same as [65]: $V_0 = 3H_0^2$, $H_0 = 10^{-5}$, $A_+ = \sqrt{\frac{9H_0^6}{4\pi^2 \times 8.5 \times 10^{-10}}}$, $A_- = A_+/1700$, $\varphi_{\text{ini}} = 1.93 \times 10^{-2}$, $\varpi_{\text{ini}} = -5.45 \times 10^{-7}$. The EOI is defined as the time when ϕ reaches $\phi_{\text{end}} = -0.0187$.

The setting of our method is as follows. Only in this test case, as the scheme for discretizing Eq. (2.2), we use not the EM scheme but a higher-degree one SRIW2 [76] in `DifferentialEquations.jl` with a finer time step size $\Delta N = 0.001$, since solving Eq. (2.2) in the USR requires the higher accuracy. n_{path} is also set to a larger value, 10^6 . We set $N_{\text{bk},l} = 10$ and $N_{\text{bk},u} = 15$. The fitting function is taken as the following one, consisting of two parts:

$$f(N_{\text{bk}}, \boldsymbol{\theta}) = \begin{cases} f_{L, N_{\text{bk},u}, N_{\text{bk},l}}^{\log}(N_{\text{bk}}, \boldsymbol{\theta}) & \text{for } N_{\text{bk}} > \theta_{-2}, \\ aN_{\text{bk}} + b & \text{otherwise,} \end{cases} \quad (4.8)$$

where

$$f_{L, N_{\text{bk},u}, N_{\text{bk},l}}^{\log}(N_{\text{bk}}, \boldsymbol{\theta}) := \frac{\theta_{-1}}{1 + \exp\left(\sum_{\ell=0}^L \theta_{\ell} p_{\ell} \left(\frac{2N_{\text{bk}} - N_{\text{bk},u} - N_{\text{bk},l}}{N_{\text{bk},u} - N_{\text{bk},l}}\right)\right)}. \quad (4.9)$$

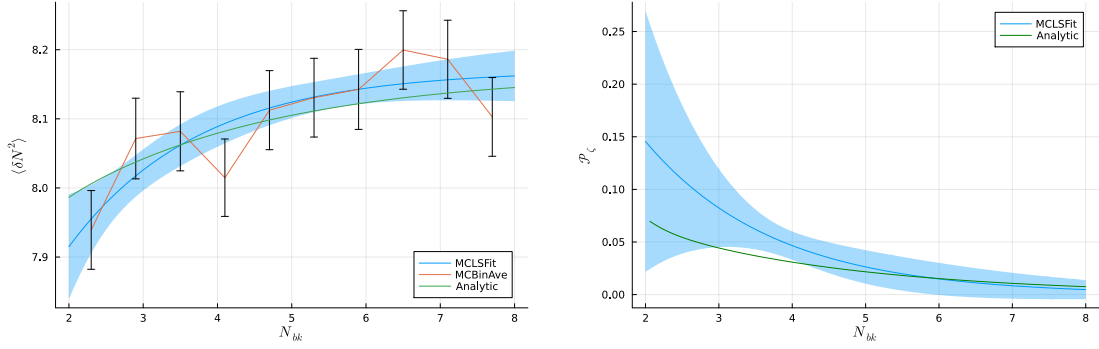


Figure 3. The same figure as FIG. 1 but for the flat quantum well model. The number of bins in MCBinAve is now 10. The analytical formulae (4.12) and (4.13) are shown in green. In the right panel, the MCBinAve result is not shown because the statistical error bar is so large that plotting the result is not illustrative.

This function has $L + 3$ tunable parameters $\theta = (\theta_{-2}, \theta_{-1}, \dots, \theta_L)$, the connection point θ_{-2} and the parameters $\theta_{-1}, \dots, \theta_L$ that determines the right part. The parameters a and b for the left part are automatically determined so that f and $\partial_{N_{bk}} f$, which correspond to $\langle \delta N^2 \rangle$ and \mathcal{P}_ζ respectively, are continuous at $N_{bk} = \theta_{-2}$. We now set $L = 4$. We will discuss this choice of the fitting function later.

The result is shown in FIG. 2. The MS-based calculation is applicable in this case [65] and its result is also shown in the figure. The USR yields a characteristic shape of \mathcal{P}_ζ : the largest peak around the point corresponding to the inflaton’s passing the potential kink and the oscillation on a flat baseline after that. MCBinAve roughly reproduces this shape, and so does MCLSFit, although the oscillation on the baseline is not captured with the current fitting function. The sample generation took 17.1 hours in this case, because of the small ΔN and large n_{path} .

We finally remark on the choice of the fitting function. We chose this by taking into account the shape of the power spectrum, specifically the large peak on the right and the otherwise flat line with oscillations on the left. In fact, the right part of f in Eq. (4.8) is based on the logistic function $1/(1 + e^{-x})$, which has a sigmoid shape, and thus its single-peaked derivative naturally fits the largest peak of \mathcal{P}_ζ . The left part of Eq. (4.8) is a linear function, whose derivative is constant. With this choice, we have obtained a function fitting the true power spectrum to some extent, as shown in FIG. 2. It may seem like a kind of cheat that we choose the fitting function knowing the true function. Although this is true, it is common and desirable to reflect prior knowledge and/or rough estimates on the true function in the machine learning context. In the current case, even if we do not know the true function, the MCBinAve estimate roughly traces its shape, suggesting a fitting function shape similar to Eq. (4.8).

4.3 Flat quantum well

The above two examples are the cases where the quantum diffusion does not dominantly determine the inflaton’s dynamics: the stochastic formalism is not necessarily required, and in fact, the MS approach works. As a third example, let us consider the flat quantum well model in AV20 [21]. This is a single-field model, in which the potential $V(\phi)$ is completely flat, namely $V(\phi) = 24\pi^2 v_{\text{well}} = \text{const}$ in the interval $[\phi_w, \phi_c]$. Thus, in this interval, there is

no potential force on the inflaton, and its dynamics is completely dominated by the quantum diffusion. At the ends of the interval, the potential is continuously connected to the non-flat parts: for $\phi < \phi_w$, $V(\phi)$ is not flat but so shallow that ϕ shows the slow-roll dynamics, and $V(\phi)$ is so steep for $\phi > \phi_c$ that ϕ_c is the EOI point.⁸ In this setting, the inflaton's dynamics is described by the following one-dimensional Langevin equation [21]

$$\frac{dx(N)}{dN} = \frac{\sqrt{2}}{\mu} \xi(N), \quad (4.10)$$

where $x(N) := (\varphi(N) - \phi_w)/(\phi_c - \phi_w)$ and $\mu = (\phi_c - \phi_w)/\sqrt{v_{\text{well}}}$. $x(N)$ has a reflective boundary at $x = 0$ and an absorbing boundary at $x = 1$, which means that $x(N)$ stops when it reaches $x = 1$, corresponding the EOI. Further, it is equivalent to the absolute value of a non-reflective process $x(N)$ that obeys Eq. (4.10) and stops when $|x(N)| = 1$. After all, to sample a total e-fold number of the inflaton's path starting from ϕ_{ini} , we may simulate $x(N)$ by Eq. (4.10) with the initial value $x_{\text{ini}} = (\phi_{\text{ini}} - \phi_w)/(\phi_c - \phi_w)$ and take the time when $x(N)$ first reaches 1 or -1 .

Practically, a naive simulation of Eq. (4.10) with this EOI condition by the EM method may not lead to accurate sampling of the first passage time in the currently considered diffusion-dominant system. For a simple problem, the first passage time of a one-dimensional Brownian motion, as we are now considering, we can use improved sampling methods developed in the field of probability theory. Specifically, we adopt the boundary shifting method proposed in Ref. [77] for a problem in mathematical finance: we reset the levels at which $x(N)$ stops as

$$\pm \left(1 - \frac{0.5826\sqrt{2\Delta N}}{\mu} \right). \quad (4.11)$$

For a more detailed explanation on this method, see Appendix A.

We compare our results in MCLSFit and MCBinAve with AV20's analytic formulae [21]:

$$\langle \delta \mathcal{N}^2 \rangle (N_{\text{bk}}) = \frac{\mu^4}{6} - \frac{8\mu^4}{3\pi^2} \sum_{n=0}^{\infty} \frac{e^{-(n+\frac{1}{2})^2 \frac{\pi^2}{\mu^2} N_{\text{bk}}}}{(n+\frac{1}{2})^2} - \frac{8\mu^4}{\pi^5} \sum_{n=0}^{\infty} \frac{e^{-(n+\frac{1}{2})^2 \frac{\pi^2}{\mu^2} N_{\text{bk}}}}{(n+\frac{1}{2})^4} \left[5 \frac{(-1)^n}{n+\frac{1}{2}} - 4\pi \right]. \quad (4.12)$$

and

$$\mathcal{P}_{\zeta}(N_{\text{bk}}) = \frac{8\mu^2}{3} \sum_{n=0}^{\infty} e^{-(n+\frac{1}{2})^2 \frac{\pi^2}{\mu^2} N_{\text{bk}}} + \frac{8\mu^2}{\pi^3} \sum_{n=0}^{\infty} \frac{e^{-(n+\frac{1}{2})^2 \frac{\pi^2}{\mu^2} N_{\text{bk}}}}{(n+\frac{1}{2})^2} \left[5 \frac{(-1)^n}{n+\frac{1}{2}} - 4\pi \right], \quad (4.13)$$

We truncate the infinite sum at $n = 10$. In particular, we would like to see the perturbation for N_{bk} larger than the expected e-folds during the quantum well phase, $\langle \mathcal{N}(x=0) \rangle = \mu^2/2$, as a very characteristic, stochastic effect reported by AV20: it corresponds to larger scales than the quantum-well scale but the stochastic effect predicts such a “leakage” of small-scale perturbations to large-scale ones.

The results of our methods for $\mu = \sqrt{7}$, corresponding to, $\langle \mathcal{N}(x=0) \rangle = 3.5$, are shown in FIG. 3, along with these analytical solutions. We set $N_{\text{bk,l}} = 3$ and $N_{\text{bk,u}} = 8$. In path

⁸Although AV20 [21] considered a more general case that ϕ can slow-roll also for $\phi > \phi_c$, we now set ϕ_c to the EOI point for simplicity as it merely shifts the scale of interest.

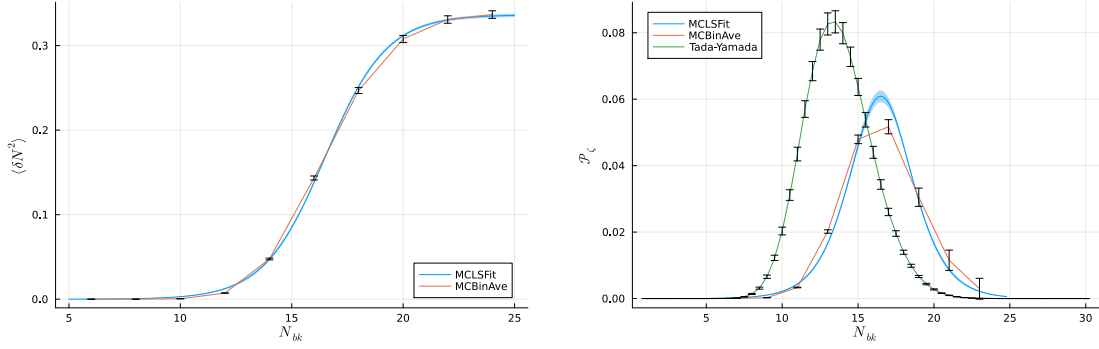


Figure 4. The same figure as FIG. 1 but for hybrid inflation. The number of bins in MCBinAve is 10. In the right panel, the power spectrum calculated by the method in Ref. [50] is shown in green.

generation, we took a finer time step size $\Delta N = 0.001$ and a larger sample size $n_{\text{path}} = 10^6$, in order to accurately reproduce the curve of $\langle \delta \mathcal{N}^2 \rangle$, which shows a larger value but a smaller relative variation than in other test cases, and to subsequently obtain \mathcal{P}_ζ . The initial point of paths should be set well before the quantum well phase to see the “leakage” effect, but we neglect the perturbation during the slow-roll phase, and hence we can set the initial point to $x_{\text{ini}} = 0$, which corresponds to the reflective boundary of the well. We found that, for a part of the paths sampled in step 3 in ALGORITHM 3, say the n -th one, its total e-fold \mathcal{N}_n was smaller than $N_{\text{bk},n}$, which made how to set $\mathbf{X}_{\text{bk},n} = x_{\text{bk},n}$, the value of x $N_{\text{bk},n}$ e-folds before the EOI, unclear. In such a case, we can again set $x_{\text{bk},n} = 0$ by neglecting the perturbation during the slow-roll phase. For fitting, we used the following function

$$f(N_{\text{bk}}, \boldsymbol{\theta}) = \theta_1 + \theta_2 \exp(\theta_3 N_{\text{bk}}) \quad (4.14)$$

with three parameters $\boldsymbol{\theta} = (\theta_1, \theta_2, \theta_3)$. We took this function shape considering the analytical formula of $\langle \delta \mathcal{N}^2 \rangle$, for which taking only the leading terms yields

$$\langle \delta \mathcal{N}^2 \rangle(N_{\text{bk}}) \simeq \frac{\mu^4}{6} - \frac{32\mu^4}{3\pi^2} \left(1 - \frac{48}{\pi^2} + \frac{120}{\pi^3} \right) e^{-\frac{\pi^2}{4\mu^2} N_{\text{bk}}}. \quad (4.15)$$

Again, this choice is also suggested by the MCBinAve result of $\langle \delta \mathcal{N}^2 \rangle$, which gradually approaches a horizontal line from below. FIG. 3 shows that although the statistical error is rather large, our estimates of $\langle \delta \mathcal{N}^2 \rangle$ and \mathcal{P}_ζ closely coincide with the true ones. The “leakage” effect for $N_{\text{bk}} > \langle \mathcal{N}(x=0) \rangle = 3.5$ can also be seen. Sample generation took 8.5 hours in this case.

Let us comment on the formulation dependence of the “leakage” effect. This effect is because the probability of $\mathcal{N}_n > N_{\text{bk},n}$ is not negligible even for $N_{\text{bk},n} > \langle \mathcal{N}(x=0) \rangle$ in such a diffusion-dominant system, and the quantum-well fluctuation can account for a part of the large-scale perturbations. This does not happen in FKTT or AV24, as they choose \mathbf{X} based on the average e-folds. In this paper, we do not discuss which formulation is correct, but we merely reproduce AV20’s result in our method based on Monte Carlo simulation and least squares fitting.

4.4 Hybrid inflation

The last example is hybrid inflation [78] with the potential

$$V(\phi) = \Lambda^4 \left[\left(1 - \frac{\psi^2}{M^2} \right)^2 + 2 \frac{\phi^2 \psi^2}{\phi_c^2 M^2} + \frac{\phi - \phi_c}{\mu_1} - \frac{(\phi - \phi_c)^2}{\mu_2^2} \right], \quad (4.16)$$

where $\Lambda, M, \mu, \phi_c > 0$ are the parameters. This model involves two fields $\phi = (\phi, \psi)$, which are usually called the inflaton and the waterfall field. Starting with the initial values $\phi_{\text{ini}} > \phi_c$ and $\psi_{\text{ini}} = 0$, ϕ rolls down with ψ kept around 0, the minimum point in the ψ direction. After it reaches ϕ_c , $\psi = 0$ becomes the local maximum point, which is called the waterfall transition, and ϕ rolls down to either of the global minima $(0, \pm M)$. Depending on the parameters, the potential around the inflection point $\phi = (\phi_c, 0)$ is very flat, and thus ϕ experiences the diffusion-dominated phase before inflation ends with $\epsilon_H = 1$. This implies that the curvature perturbation of a scale that exits the Hubble horizon around the waterfall transition may be greatly enhanced, as explored in, e.g., Refs. [19, 23, 50, 57, 79–86].

Now, as in Ref. [58], we set the model parameters as

$$M = \frac{\phi_c}{\sqrt{2}} = 10^{16} \text{ GeV}, \quad \mu_1 = \frac{100}{M^2 \phi_c}, \quad \mu_2 = 10, \quad \Lambda = 5.4 \times 10^{15} \text{ GeV} \times M \phi_c^{1/2}, \quad (4.17)$$

and the initial values

$$(\phi_{\text{ini}}, \boldsymbol{\pi}_{\text{ini}}) = (\phi_{\text{ini}}, \psi_{\text{ini}}, 0, 0), \quad (4.18)$$

where

$$\phi_{\text{ini}} = \phi_c + \frac{15}{\mu_1}, \quad \psi_{\text{ini}} = \sqrt{\frac{5\Lambda^4}{24\sqrt{2}\pi^3}}. \quad (4.19)$$

For each field, the noise power spectrum is set as $\mathcal{P}_\phi = \mathcal{P}_\psi = \frac{H}{2\pi}$. The EOI is set to the moment when $\partial_\psi^2 V/V = -2$. For the setting of our method, we set $N_{\text{bk},l} = 5$ and $N_{\text{bk},u} = 25$ and take the fitting function $f(N_{\text{bk}}, \boldsymbol{\theta}) = f_{L, N_{\text{bk},u}, N_{\text{bk},l}}^{\text{log}}(N_{\text{bk}}, \boldsymbol{\theta})$, a logistic function with a polynomial inside, which was also used in Sec. 4.2. We chose this function because of the knowledge that \mathcal{P}_ζ has a single large peak; the derivative of a logistic function has such a shape. We now set $L = 2$.

We show the result of our method in FIG. 4. Now, the MS-based result is not accompanied because the perturbed approach breaks down in this model. MCLSFit produces $\tilde{\mathcal{P}}_\zeta$ having a peak with small statistical errors. The result of MCBinAve almost fits this, with the peak height somewhat suppressed due to its averaging nature.

For the sake of comparison, we also plot \mathcal{P}_ζ calculated by the method proposed by Tada and Yamada (TY) [50], based on the adjoint Fokker–Planck PDE described in Sec. 3.4. Except for several tens of percent differences in the position and the height of the peak, their qualitative features agree with each other. Quantitative differences may arise from the fact that TY took the slow-roll approximation to neglect the velocities $\boldsymbol{\varpi}$. In this test case, our code took 9.8 minutes for sample generation, while TY’s programme takes around 40 minutes in addition to 6 minutes to solve the PDEs (by M1 Max MacBook Pro), though TY’s sample generation would also be improved by utilizing a public library.

5 Summary

In this paper, we proposed novel algorithms to calculate the inflationary curvature perturbation power spectrum \mathcal{P}_ζ in the stochastic- $\delta\mathcal{N}$ formalism. To deal with multi-field inflation models, some kind of numerical approach is desired, but existing Monte Carlo-based methods are computationally demanding due to their nested structure. Our proposal makes improvements twofold. First, we avoid nested Monte Carlo simulation by taking an estimator (3.6) of $\langle\delta\mathcal{N}_\mathbf{X}^2\rangle$, which can be calculated by generating just two branches from each path. This largely reduces the number of paths generated in the simulation. Second, we incorporate least squares curve fitting into this Monte Carlo-based method: we perform fitting of a certain parametric function to data sampled in Monte Carlo path generation. Then, our method does not need to estimate \mathcal{P}_ζ at a finite number n_{PS} of scales, and its computational cost is not proportional to n_{PS} . Rather, our method produces an approximating function of \mathcal{P}_ζ over a range of scales with a reduced computational cost. We also conduct numerical demonstrations of our method in some inflation models. The results imply that, although the choice of fitting function can be an issue, especially when \mathcal{P}_ζ has a complicated shape, our method works in various cases, including hybrid inflation.

Although we take only the power spectrum as a target in this paper, it would be interesting to extend our method to calculating higher-order statistics. For example, since

$$\langle\delta\mathcal{N}_\mathbf{X}^3\rangle = \left\langle \frac{1}{6} \left(2\mathcal{N}_\mathbf{X}^{(1)} - \mathcal{N}_\mathbf{X}^{(2)} - \mathcal{N}_\mathbf{X}^{(3)} \right)^3 \right\rangle \quad (5.1)$$

holds, where $\mathcal{N}_\mathbf{X}^{(1,2,3)}$ are e-folds of three independent paths starting from the point \mathbf{X} , we have an estimator of $\langle\delta\mathcal{N}_\mathbf{X}^3\rangle$ that can be calculated via generating just three branches. If we could find some formula like Eq. (2.9) that connects $\langle\delta\mathcal{N}_\mathbf{X}^3\rangle$ to the bispectrum of the curvature perturbation, we could build a similar method for the bispectrum. We will consider such a possibility in future work.

Acknowledgements

KM is supported by MEXT Quantum Leap Flagship Program (MEXT Q-LEAP) Grant no. JPMXS0120319794, and JST COI-NEXT Program Grant No. JPMJPF2014. YT is supported by JSPS KAKENHI Grant No. JP24K07047.

A Boundary shifting

The task considered in Sec. 4.3 is a kind of first-passage problem for a Brownian motion. Let us consider a random process $X(t)$ obeying the following Langevin equation

$$\frac{dX(t)}{dt} = \sigma\xi(t) \quad (\text{A.1})$$

with a constant $\sigma > 0$ and the initial value $X(0) = 0$, or, equivalently, the following stochastic differential equation

$$dX(t) = \sigma dW(t), \quad (\text{A.2})$$

where $W(t)$ is a Brownian motion. Then, we consider the time τ when X first exceeds the value B ,

$$\tau_B := \inf \{t > 0 \mid X(t) \geq B\}, \quad (\text{A.3})$$

where B is assumed to be positive without loss of generality. To analyze the distribution of τ , the approach taken in Sec. 4.3 is the Monte Carlo-based one: we generate paths of X and take

$$\tilde{\tau}_B = \inf \{t_j \mid X(t_j) \geq B\}, \quad (\text{A.4})$$

as an approximation of τ_B . Here, although X is originally continuous in time, generated paths are inevitably discrete: we assume that each of them consists of $X(t_1), \dots, X(t_n)$, where $t_i := i\Delta t$ is the i -th time grid point with an interval Δt . Then, this causes the issue of discrete observation. For a path, if all the $X(t_1), \dots, X(t_n)$ are below B , we consider that this path did not exceed B . However, such a path might actually exceed B at some time between t_i and t_{i+1} . We are neglecting such an event, which leads to underestimating the probability of X reaching B and overestimating τ_B : according to Ref. [77], the difference between the distributions of τ_B and $\tilde{\tau}_B$ scales as

$$|\Pr(\tilde{\tau}_B \leq t_i) - \Pr(\tau_B \leq t_i)| = O(\sqrt{\Delta t}). \quad (\text{A.5})$$

Coping with the difference between the discrete first-passage problem and the continuous one has been studied in the field of probability theory, especially mathematical finance. A simple way is shifting the boundary, which was proposed in Ref. [77] based on Ref. [87]. Because the first-passage probability is higher for a lower B , lowering B pushes the probability underestimated by the discrete observation to the true value. According to Ref. [77], by resetting B to

$$\tilde{B} := B - \beta\sigma\sqrt{\Delta t}, \quad \beta := -\frac{\zeta\left(\frac{1}{2}\right)}{\sqrt{2\pi}} \simeq 0.5826, \quad (\text{A.6})$$

where ζ is the Riemann zeta function, the first-passage probability with discrete observation is approximately modified to the continuous one:

$$|\Pr(\tilde{\tau}_B \leq t_i) - \Pr(\tau_B \leq t_i)| = o(\sqrt{\Delta t}). \quad (\text{A.7})$$

References

- [1] A.A. Starobinsky, *Multicomponent de Sitter (Inflationary) Stages and the Generation of Perturbations*, *JETP Lett.* **42** (1985) 152.
- [2] D.S. Salopek and J.R. Bond, *Nonlinear evolution of long wavelength metric fluctuations in inflationary models*, *Phys. Rev. D* **42** (1990) 3936.
- [3] M. Sasaki and E.D. Stewart, *A General analytic formula for the spectral index of the density perturbations produced during inflation*, *Prog. Theor. Phys.* **95** (1996) 71 [[astro-ph/9507001](#)].
- [4] D. Wands, K.A. Malik, D.H. Lyth and A.R. Liddle, *A New approach to the evolution of cosmological perturbations on large scales*, *Phys. Rev. D* **62** (2000) 043527 [[astro-ph/0003278](#)].
- [5] D.H. Lyth, K.A. Malik and M. Sasaki, *A General proof of the conservation of the curvature perturbation*, *JCAP* **05** (2005) 004 [[astro-ph/0411220](#)].
- [6] A.A. Starobinsky, *Dynamics of Phase Transition in the New Inflationary Universe Scenario and Generation of Perturbations*, *Phys. Lett. B* **117** (1982) 175.
- [7] A.A. Starobinsky, *STOCHASTIC DE SITTER (INFLATIONARY) STAGE IN THE EARLY UNIVERSE*, *Lect. Notes Phys.* **246** (1986) 107.

- [8] Y. Nambu and M. Sasaki, *Stochastic Stage of an Inflationary Universe Model*, *Phys. Lett. B* **205** (1988) 441.
- [9] Y. Nambu and M. Sasaki, *Stochastic approach to chaotic inflation and the distribution of universes*, *Phys. Lett. B* **219** (1989) 240.
- [10] H.E. Kandrup, *STOCHASTIC INFLATION AS A TIME DEPENDENT RANDOM WALK*, *Phys. Rev. D* **39** (1989) 2245.
- [11] K.-i. Nakao, Y. Nambu and M. Sasaki, *Stochastic Dynamics of New Inflation*, *Prog. Theor. Phys.* **80** (1988) 1041.
- [12] Y. Nambu, *Stochastic Dynamics of an Inflationary Model and Initial Distribution of Universes*, *Prog. Theor. Phys.* **81** (1989) 1037.
- [13] S. Mollerach, S. Matarrese, A. Ortolan and F. Lucchin, *Stochastic inflation in a simple two field model*, *Phys. Rev. D* **44** (1991) 1670.
- [14] D.S. Salopek and J.R. Bond, *Stochastic inflation and nonlinear gravity*, *Phys. Rev. D* **43** (1991) 1005.
- [15] A.D. Linde, D.A. Linde and A. Mezhlumian, *From the Big Bang theory to the theory of a stationary universe*, *Phys. Rev. D* **49** (1994) 1783 [[gr-qc/9306035](#)].
- [16] A.A. Starobinsky and J. Yokoyama, *Equilibrium state of a selfinteracting scalar field in the De Sitter background*, *Phys. Rev. D* **50** (1994) 6357 [[astro-ph/9407016](#)].
- [17] D. Cruces, *Review on Stochastic Approach to Inflation*, *Universe* **8** (2022) 334 [[2203.13852](#)].
- [18] T. Fujita, M. Kawasaki, Y. Tada and T. Takesako, *A new algorithm for calculating the curvature perturbations in stochastic inflation*, *JCAP* **12** (2013) 036 [[1308.4754](#)].
- [19] T. Fujita, M. Kawasaki and Y. Tada, *Non-perturbative approach for curvature perturbations in stochastic δN formalism*, *JCAP* **10** (2014) 030 [[1405.2187](#)].
- [20] V. Vennin and A.A. Starobinsky, *Correlation Functions in Stochastic Inflation*, *Eur. Phys. J. C* **75** (2015) 413 [[1506.04732](#)].
- [21] K. Ando and V. Vennin, *Power spectrum in stochastic inflation*, *JCAP* **04** (2021) 057 [[2012.02031](#)].
- [22] C. Animali and V. Vennin, *Clustering of primordial black holes from quantum diffusion during inflation*, *JCAP* **08** (2024) 026 [[2402.08642](#)].
- [23] M. Kawasaki and Y. Tada, *Can massive primordial black holes be produced in mild waterfall hybrid inflation?*, *JCAP* **08** (2016) 041 [[1512.03515](#)].
- [24] H. Assadullahi, H. Firouzjahi, M. Noorbala, V. Vennin and D. Wands, *Multiple Fields in Stochastic Inflation*, *JCAP* **06** (2016) 043 [[1604.04502](#)].
- [25] V. Vennin, H. Assadullahi, H. Firouzjahi, M. Noorbala and D. Wands, *Critical Number of Fields in Stochastic Inflation*, *Phys. Rev. Lett.* **118** (2017) 031301 [[1604.06017](#)].
- [26] C. Pattison, V. Vennin, H. Assadullahi and D. Wands, *Quantum diffusion during inflation and primordial black holes*, *JCAP* **10** (2017) 046 [[1707.00537](#)].
- [27] J.M. Ezquiaga and J. García-Bellido, *Quantum diffusion beyond slow-roll: implications for primordial black-hole production*, *JCAP* **08** (2018) 018 [[1805.06731](#)].
- [28] M. Noorbala, V. Vennin, H. Assadullahi, H. Firouzjahi and D. Wands, *Tunneling in Stochastic Inflation*, *JCAP* **09** (2018) 032 [[1806.09634](#)].
- [29] H. Firouzjahi, A. Nassiri-Rad and M. Noorbala, *Stochastic Ultra Slow Roll Inflation*, *JCAP* **01** (2019) 040 [[1811.02175](#)].

- [30] M. Noorbala and H. Firouzjahi, *Boundary crossing in stochastic inflation with a critical number of fields*, *Phys. Rev. D* **100** (2019) 083510 [[1907.13149](#)].
- [31] N. Kitajima, Y. Tada and F. Takahashi, *Stochastic inflation with an extremely large number of e-folds*, *Phys. Lett. B* **800** (2020) 135097 [[1908.08694](#)].
- [32] T. Prokopec and G. Rigopoulos, ΔN and the stochastic conveyor belt of ultra slow-roll inflation, *Phys. Rev. D* **104** (2021) 083505 [[1910.08487](#)].
- [33] J.M. Ezquiaga, J. García-Bellido and V. Vennin, *The exponential tail of inflationary fluctuations: consequences for primordial black holes*, *JCAP* **03** (2020) 029 [[1912.05399](#)].
- [34] H. Firouzjahi, A. Nassiri-Rad and M. Noorbala, *Stochastic nonattractor inflation*, *Phys. Rev. D* **102** (2020) 123504 [[2009.04680](#)].
- [35] A. De and R. Mahbub, *Numerically modeling stochastic inflation in slow-roll and beyond*, *Phys. Rev. D* **102** (2020) 123509 [[2010.12685](#)].
- [36] D.G. Figueroa, S. Raatikainen, S. Rasanen and E. Tomberg, *Non-Gaussian Tail of the Curvature Perturbation in Stochastic Ultraslow-Roll Inflation: Implications for Primordial Black Hole Production*, *Phys. Rev. Lett.* **127** (2021) 101302 [[2012.06551](#)].
- [37] C. Pattison, V. Vennin, D. Wands and H. Assadullahi, *Ultra-slow-roll inflation with quantum diffusion*, *JCAP* **04** (2021) 080 [[2101.05741](#)].
- [38] D.G. Figueroa, S. Raatikainen, S. Rasanen and E. Tomberg, *Implications of stochastic effects for primordial black hole production in ultra-slow-roll inflation*, *JCAP* **05** (2022) 027 [[2111.07437](#)].
- [39] Y. Tada and V. Vennin, *Statistics of coarse-grained cosmological fields in stochastic inflation*, *JCAP* **02** (2022) 021 [[2111.15280](#)].
- [40] J.M. Ezquiaga, J. García-Bellido and V. Vennin, *Massive Galaxy Clusters Like El Gordo Hint at Primordial Quantum Diffusion*, *Phys. Rev. Lett.* **130** (2023) 121003 [[2207.06317](#)].
- [41] N. Ahmadi, M. Noorbala, N. Feyzabadi, F. Eghbalpoor and Z. Ahmadi, *Quantum diffusion in sharp transition to non-slow-roll phase*, *JCAP* **08** (2022) 078 [[2207.10578](#)].
- [42] A. Nassiri-Rad, K. Asadi and H. Firouzjahi, *Inflation with stochastic boundary*, *Phys. Rev. D* **106** (2022) 123528 [[2208.08229](#)].
- [43] C. Animalì and V. Vennin, *Primordial black holes from stochastic tunnelling*, *JCAP* **02** (2023) 043 [[2210.03812](#)].
- [44] E. Tomberg, *Numerical stochastic inflation constrained by frozen noise*, *JCAP* **04** (2023) 042 [[2210.17441](#)].
- [45] A.D. Gow, H. Assadullahi, J.H.P. Jackson, K. Koyama, V. Vennin and D. Wands, *Non-perturbative non-Gaussianity and primordial black holes*, *EPL* **142** (2023) 49001 [[2211.08348](#)].
- [46] G. Rigopoulos and A. Wilkins, *Computing first-passage times with the functional renormalisation group*, *JCAP* **04** (2023) 046 [[2211.09649](#)].
- [47] V. Briaud and V. Vennin, *Uphill inflation*, *JCAP* **06** (2023) 029 [[2301.09336](#)].
- [48] K. Asadi, A. Nassiri-Rad and H. Firouzjahi, *Stochastic multiple fields inflation: Diffusion dominated regime*, *Phys. Rev. D* **108** (2023) 123537 [[2304.00577](#)].
- [49] E. Tomberg, *Stochastic constant-roll inflation and primordial black holes*, *Phys. Rev. D* **108** (2023) 043502 [[2304.10903](#)].
- [50] Y. Tada and M. Yamada, *Stochastic dynamics of multi-waterfall hybrid inflation and formation of primordial black holes*, *JCAP* **11** (2023) 089 [[2306.07324](#)].

- [51] K. Tokeshi and V. Vennin, *Why Does Inflation Look Single Field to Us?*, *Phys. Rev. Lett.* **132** (2024) 251001 [[2310.16649](#)].
- [52] S. Raatikainen, S. Räsänen and E. Tomberg, *Primordial Black Hole Compaction Function from Stochastic Fluctuations in Ultraslow-Roll Inflation*, *Phys. Rev. Lett.* **133** (2024) 121403 [[2312.12911](#)].
- [53] K. Miyamoto and Y. Tada, *Improved quantum algorithm for calculating eigenvalues of differential operators and its application to estimating the decay rate of the perturbation distribution tail in stochastic inflation*, *Phys. Rev. Res.* **7** (2025) 023251 [[2410.02276](#)].
- [54] K. Tokeshi, *Curvaton distribution from stochastic inflation*, *JCAP* **06** (2025) 018 [[2411.15849](#)].
- [55] T. Kuroda, A. Naruko, V. Vennin and M. Yamaguchi, “Primordial black holes from a curvaton: the role of bimodal distributions.” 4, 2025.
- [56] T. Takahashi and K. Tokeshi, “More fields are different: Stochastic view of multi-field inflationary scenario.” 4, 2025.
- [57] Y. Tada and M. Yamada, *Primordial black hole formation in hybrid inflation*, *Phys. Rev. D* **107** (2023) 123539 [[2304.01249](#)].
- [58] Y. Tada and M. Yamada, *Multifield stochastic dynamics in GUT hybrid inflation without monopole problem and with gravitational wave signatures of GUT Higgs representation*, *Phys. Lett. B* **855** (2024) 138854 [[2405.08859](#)].
- [59] L. Pinol, S. Renaux-Petel and Y. Tada, *A manifestly covariant theory of multifield stochastic inflation in phase space: solving the discretisation ambiguity in stochastic inflation*, *JCAP* **04** (2021) 048 [[2008.07497](#)].
- [60] F. Finelli, G. Marozzi, A.A. Starobinsky, G.P. Vacca and G. Venturi, *Generation of fluctuations during inflation: Comparison of stochastic and field-theoretic approaches*, *Phys. Rev. D* **79** (2009) 044007 [[0808.1786](#)].
- [61] F. Finelli, G. Marozzi, A.A. Starobinsky, G.P. Vacca and G. Venturi, *Stochastic growth of quantum fluctuations during slow-roll inflation*, *Phys. Rev. D* **82** (2010) 064020 [[1003.1327](#)].
- [62] C. Pattison, V. Vennin, H. Assadullahi and D. Wands, *Stochastic inflation beyond slow roll*, *JCAP* **07** (2019) 031 [[1905.06300](#)].
- [63] J. Tokuda and T. Tanaka, *Statistical nature of infrared dynamics on de Sitter background*, *JCAP* **02** (2018) 014 [[1708.01734](#)].
- [64] J. Tokuda and T. Tanaka, *Can all the infrared secular growth really be understood as increase of classical statistical variance?*, *JCAP* **11** (2018) 022 [[1806.03262](#)].
- [65] Y. Mizuguchi, T. Murata and Y. Tada, *STOLAS: STOchastic LAttice Simulation of cosmic inflation*, *JCAP* **12** (2024) 050 [[2405.10692](#)].
- [66] G. Maruyama, *Continuous markov processes and stochastic equations*, *Rend. Circ. Mat. Palermo* **4** (1955) 48.
- [67] L. Györfi, M. Kohler, A. Krzyzak and H. Walk, *A distribution-free theory of nonparametric regression*, Springer Science & Business Media (2006), [10.1007/b97848](#).
- [68] P.C. Hansen, V. Pereyra and G. Scherer, *Least squares data fitting with applications*, JHU Press (2013).
- [69] T. Murata and Y. Tada.
- [70] C. Animalì, P. Auclair, B. Blachier and V. Vennin, *Harvesting primordial black holes from stochastic trees with FOREST*, *JCAP* **05** (2025) 019 [[2501.05371](#)].
- [71] C. Rackauckas and Q. Nie, *DifferentialEquations.jl—a performant and feature-rich ecosystem for solving differential equations in Julia*, *Journal of Open Research Software* **5** (2017) .

- [72] A.D. Linde, *Chaotic Inflation*, *Phys. Lett. B* **129** (1983) 177.
- [73] “Lsqfit.jl.”
- [74] A.A. Starobinsky, *Spectrum of adiabatic perturbations in the universe when there are singularities in the inflation potential*, *JETP Lett.* **55** (1992) 489.
- [75] S. Pi and J. Wang, *Primordial black hole formation in Starobinsky’s linear potential model*, *JCAP* **06** (2023) 018 [[2209.14183](#)].
- [76] A. Rößler, *Runge–kutta methods for the strong approximation of solutions of stochastic differential equations*, *SIAM Journal on Numerical Analysis* **48** (2010) 922.
- [77] M. Broadie, P. Glasserman and S. Kou, *A continuity correction for discrete barrier options*, *Mathematical Finance* **7** (1997) 325.
- [78] A.D. Linde, *Hybrid inflation*, *Phys. Rev. D* **49** (1994) 748 [[astro-ph/9307002](#)].
- [79] J. Garcia-Bellido, A.D. Linde and D. Wands, *Density perturbations and black hole formation in hybrid inflation*, *Phys. Rev. D* **54** (1996) 6040 [[astro-ph/9605094](#)].
- [80] D.H. Lyth, *Contribution of the hybrid inflation waterfall to the primordial curvature perturbation*, *JCAP* **07** (2011) 035 [[1012.4617](#)].
- [81] E. Bugaev and P. Klimai, *Curvature perturbation spectra from waterfall transition, black hole constraints and non-Gaussianity*, *JCAP* **11** (2011) 028 [[1107.3754](#)].
- [82] E. Bugaev and P. Klimai, *Formation of primordial black holes from non-Gaussian perturbations produced in a waterfall transition*, *Phys. Rev. D* **85** (2012) 103504 [[1112.5601](#)].
- [83] D.H. Lyth, *The hybrid inflation waterfall and the primordial curvature perturbation*, *JCAP* **05** (2012) 022 [[1201.4312](#)].
- [84] A.H. Guth and E.I. Sfakianakis, “Density Perturbations in Hybrid Inflation Using a Free Field Theory Time-Delay Approach.” 10, 2012.
- [85] I.F. Halpern, M.P. Hertzberg, M.A. Joss and E.I. Sfakianakis, *A Density Spike on Astrophysical Scales from an N-Field Waterfall Transition*, *Phys. Lett. B* **748** (2015) 132 [[1410.1878](#)].
- [86] S. Clesse and J. García-Bellido, *Massive Primordial Black Holes from Hybrid Inflation as Dark Matter and the seeds of Galaxies*, *Phys. Rev. D* **92** (2015) 023524 [[1501.07565](#)].
- [87] D. Siegmund and Y.-S. Yuh, *Brownian approximations to first passage probabilities*, *Zeitschrift für Wahrscheinlichkeitstheorie und verwandte Gebiete* **59** (1982) 239.